OPTICAL STUDY OF THE ELECTRONIC BAND STRUCTURE OF DIAMOND

by

Richard Arthur Roberts

Technical Report

National Aeronautics and Space Administration
Research Grant #NSG 91-60 Supplement #4

January 1967

Principal Investigator: William C. Walker,
Associate Professor of Physics
University of California, Santa Barbara

ABSTRACT

Optical Study of the Electronic Band Structure of Diamond

by

Richard Arthur Roberts

Absolute normal incidence reflection measurements at both room and liquid nitrogen temperatures have been taken on a polished Type I and both cleaved and polished Type IIa diamond crystals in the range from 5.5 to 11.5 eV. A Vacion pumping system was used in the low temperature work to eliminate oil contamination of the crystal surface. Additional room temperature measurements up to 31 eV were made on the polished Type I and cleaved Type IIa crystals.

The Kramers-Kronig analysis used in this research to determine the phase angle differs from previous work in as much as no extrapolation of data outside the measured high energy limit was required. The dielectric function $\hat{\epsilon}$ was obtained over a broad energy range (5.5 - 31 eV) and structure was observed at 7.3, 7.8, 12.2 and 23 eV. The 7.3 and 12.2 peaks, assigned to direct interband transitions on the basis of recent band calculations, are in agreement with earlier measurements. Evidence that the 23 eV peak is not intrinsic to diamond is presented. New low temperature observations on the absorption threshold indicate that the previously suggested model based on a hybrid exciton is probably incorrect. The conclusion of this research is that the direct

band edge is near 7.3 eV. The previously unobserved temperature dependent 7.8 eV peak can be explained as due to a change in the energy bands near the Γ point although an exciton interpretation is not excluded.

Agreement of the present research with the latest previous measurement is remarkably good considering that different samples and methods of analysis were used.

LIST OF FIGURES

TABLE OF CONTENTS

I. INTRODUCTION

Detailed analysis of optical spectra has provided the most important means of arriving at an accurate description of the electronic structure of free atoms and molecules. Until recently the use of fundamental optical spectra to study the electronic structure of the solid state had been thwarted by (a) lack of suitable spectra for analysis, and (b) lack of a guiding theoretical scheme for interpretation of the spectra.

For insulating materials the electronic states within 1 eV of the valence band maximum or conduction band minimum (band edges) may be called infrared states in contrast to ultraviolet states which refer to those states within 1 to 10 eV of the band edges. Until 1959 most experimental studies were confined to the infrared states using infrared absorption, de Haas-van Alphen or cyclotron resonance techniques. These experiments give the electron effective mass which in turn gives information about the shape of the band edges. From a theoretical point of view this was unsatisfactory as band calculations give all the electronic states over as much as 30 eV from the edges.

Philipp and Taft[1] were the first to extend the measurements over a broader range of energy. They examined the ultraviolet spectra of Ge and Si crystals, whose infrared states had been extensively studied, by making reflection measurements over the range from 1 to 10 eV. Using the Kramers-Kronig relations they derived ε_1 and ε_2, the components of the complex dielectric function, over the same energy range.

Phillips[2] realized that if the interband oscillator strength occurring in the theoretical expression for ε_2 varies smoothly with $\vec{k}$ then the structure in ε_2 is due to singularities in the electronic joint density of states function. By examining the theoretical energy bands he introduced the concept of critical points in the joint density of states as the source of singularities and hence structure in ε_2. This concept, which is now well accepted, provides the necessary framework for interpretation of the electronic spectra of solids.

Most electron energy band calculations are based on the Bloch model of a solid which assumes electrons moving independently through a periodic potential. This model has been our most useful theoretical tool, but, in fact, electrons are not independent and in many cases their interactions cannot be neglected. Many-body problems are inherently difficult theoretically and their effect is generally treated as a perturbation of the Bloch model. Various theoretical approximations are in use today and experiments are crucial in determining which approximations are valid. Reliable experiments are also important because the most accurate band calculations using the Bloch model rely on making a parametric fit with experimental data.

In this research the optical constants of diamond, in the energy range from 5.5 - 11.5 eV at liquid nitrogen temperature and from 5.5 - 31 eV at room temperature, were obtained by reflectance measurements using the Kramers-Kronig analysis. The results were interpreted in terms of recent band structure calculations.

The extensive work done on silicon and germanium makes the study of diamond a logical step, as carbon is the first element in the same column as Ge and Si. Since the diamond crystal structure and covalent bonding is common to all three materials, interpretation of spectral results on diamond can rely heavily on the information obtained for Ge and Si.

Diamond is of especial theoretical interest bacause of all the covalent materials it should have the simplest and most basic structure. In addition, the accuracy of band calculations, affected by the uncertainty in the atomic electron core potential, should be greatest for diamond whose core contains only the completed 1s shell.

The present work differs from earlier efforts in several respects. Both low temperature and room temperature measurements were extended to higher photon energy. This extension is significant because of the controversy existing over possible structure occurring in these regions. In addition considerable care was taken to ensure cleanliness of the sample surface during low temperature measurements. This was accomplished by evacuating the reflectometer separately from the monochromator using a Vacion pumping system thus avoiding likely contamination of the crystal surface by diffusion pump oil. By using improved resolution a higher density of data points was obtained than in previous work thus giving more reliable information about fine structure in reflectance.

II. REVIEW OF PREVIOUS RESEARCH ON DIAMOND

A. GENERAL PROPERTIES

X-ray diffraction has shown the crystal structure of diamond to be cubic. The structure can be considered as two interpenetrating fcc crystals with origins at (0,0,0) and $(\frac{1}{4},\frac{1}{4},\frac{1}{4})$. The lattic constant or cube edge is 3.57 Å and the nearest neighbor separation is 1.54 Å. The electronic configuration of the carbon atom is $1s^2 2s^2 2p^2$ and in the crystal the inner core K electrons remain relatively undisturbed while the four L electrons pair up with nearest neighbor electrons to form tetrahedrally oriented covalent bonds.

In 1934 Robertson et al.[3,4] reported marked differences in the optical and photoconductive properties of various diamond specimens. They classified diamonds into Type I or Type II according to their different ultraviolet and infrared absorption properties. The rarer Type II diamond (approximately 5% of those occurring naturally) has infrared absorption bands between 3 and 6 μ and a sharp absorption edge near 2250 Å. For Type I diamonds the absorption edge occurs near 3000 Å and additional infrared absorption bands exist. The Type II diamonds can be further subdivided into Types IIa and IIb where those classified as Type IIb were found to have a pronounced electrical conductivity and showed phosphorescence when illuminated by ultraviolet radiation.

Kaiser and Bond[5] found nitrogen concentrations as high as 4×10^{20} nitrogen atoms per cm^3 in diamonds of Type I. Density measurements

indicated that the nitrogen occupies a substitutional position in the diamond lattice. Kaiser and Bond quantitatively showed that the nitrogen content could be correlated with the Type I characteristics; namely, additional infrared absorption near 8μ, the ultraviolet absorption above 2250 Å, and the larger lattice constant. Other impurities are present but not in sufficient concentration to account for the optical or electrical properties characteristic of Type I diamonds.

The sharp rise in the ultraviolet absorption of Type II diamonds at 2250 Å (5.6 eV) is considered as the true absorption edge of pure diamond. The shift in absorption to longer wavelengths is proportional to the nitrogen concentration and thus the absorption of Type I diamonds for $\lambda > 2250$ Å must be considered as an extrinsic tail on the true intrinsic absorption edge of diamond.

B. ELECTRONIC STATE CALCULATIONS

The first energy band calculation of diamond was done by Herman[6] in 1954, using the method of orthogonalized plane waves first proposed by Herring.[7] He found the maximum in the valence band to be at the center of the Brillouin zone or Γ point while the minimum in the conduction band was not at Γ but part way along the [1,0,0] direction.

Kleinman and Phillips[8] showed that Herman's results were nearly self consistent. By an alternate calculation procedure using an "effective potential" they found results in close agreement with those of Herman.

In 1962 Redei[9] calculated the conduction band in diamond by expanding its eigenfunctions in terms of plane waves made orthogonal to the 1s band (OPW method) and the valence band. The minimum in the conduction band was found to be about halfway along the [1,0,0] direction.

In order to confirm the OPW band calculations by an alternate method Cohan, Pugh, and Tredgold[10] worked out the valence and conduction bands in diamond by a tight-binding procedure. The general shape of the bands from this tight-binding method agreed with the OPW calculations but the width of the valence band, 52 eV, and the energy gap, 9.8 eV, were too large in comparison with experiment. These workers found both the top of the valence band and the bottom of the conduction band located at the center of the zone contrary to previous calculations.

Recently (1966) Saslow, Bergstresser and Cohen[11] (SBC) using an Empirical Pseudopotential Method made yet another band calculation. This method uses experimental results to calculate the bands. For example in diamond the experimentally determined lattice constant of 3.57 $\mathring{A}$, the conduction band minimum of 5.48 eV at (0.77,0,0) and the 12.9 eV separation of $X_4 \rightarrow X_1$ were used. Several critical points were found in the neighborhood of Γ.

In a paper presented at the International Conference on the Physics of Semiconductors, Herman[12] and others presented a new band structure obtained by adding small empirical corrections to a first principles calculation. The theoretical model was adjusted to give the experimental indirect gap of $\Gamma_{25'} \rightarrow \Delta_1 = 5.47$ eV.

For reference purposes and further discussion in following chapters the most recent band calculations are presented in Figure 1 which shows a comparison of Herman's work with that of SBC.

C. INTRINSIC OPTICAL PROPERTIES AND ELECTRONIC STRUCTURE

The extensive literature dealing with the infrared and visible optical properties of diamond has been summarized in a monograph by Champion.[13] Although these studies are useful in understanding many impurity sensitive phenomena they have not shed much light on the fundamental problem of the electronic structure of diamond.

The first optical study of the intrinsic diamond spectrum was that of Philipp and Taft.[14] They determined the optical constants and, in particular, ϵ_2 in the range 5.5 to 23 eV by Kramers-Kronig analysis of room temperature normal incidence reflectance data. Structure in ϵ_2 near 7 and 12 eV was observed and by consideration of band shape and similarity of features to that of Si which had been rather completely interpreted, and 7 and 12 eV peaks were analogously associated with direct transitions $\Gamma_{25'} \rightarrow \Gamma_{15}$ at the center of the Brillouin zone and $X_4 \rightarrow X_1$ at $\vec{k} = \frac{2\pi}{a}(100)$ respectively.

A later study in 1963 by Walker and Osantowski[15] of the absolute reflectance spectrum of a Type II specimen at room temperature from 4 to 30 eV showed structure in ϵ_2 near 7, 12, 16, 20 and 24 eV. The 7 and 12 eV peaks were given the same interpretation as that of Philipp and Taft.[13] The new high energy structure near 16, 20, and 24 eV was assigned to transitions near the L point $\vec{k} = (111)$ of the Brillouin zone.

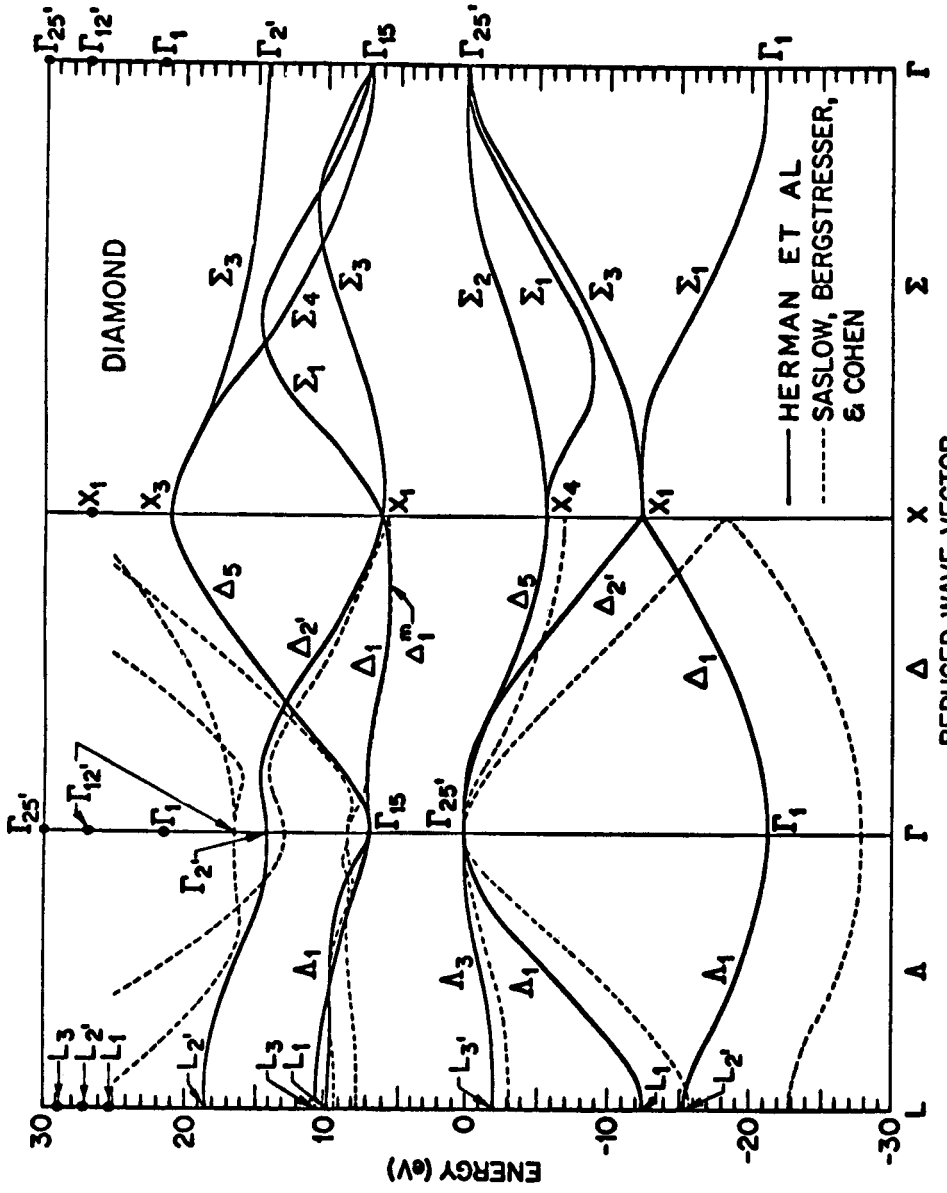

Fig. 1. Comparison of two energy band models for diamond.

The existence of the new structure which was not seen by Philipp and Taft[14] was explained as possibly originating from the increased purity of the sample used by Walker and Osantowski.[15]

Clark, Dean and Harris[16] (CDH) in 1963 performed extensive transmission studies on the indirect intrinsic absorption edge in diamond and also recorded the reflection spectrum between 5 and 14 eV at room temperature and between 5 and 8 eV at 133°K. They observed peaks at 7 and 12.5 eV and an additional weaker peak at 9 eV. At the lower temperature they observed the 7 eV peak to be sharper and more intense and shifted slightly to a higher energy as compared to the room temperature results. In addition, the reflectance at low temperature was observed to drop below the room temperature result beyond 7.5 eV. The 9 eV peak was assumed to arise from threshold transitions at the L point. According to CDH the temperature dependence of the 7 eV peak was

$$\frac{dE_g(\text{direct})}{dT} = -6.3 \pm 1.8 \times 10^{-4} \text{ eV/degK.} \qquad (1)$$

Philipp and Taft[17] remeasured diamond and obtained a new reflectance curve which differed only slightly from their previous measurement. They did, however, observe structure near 24 eV not resolved earlier. A reanalysis of Walker and Osantowski's[15] data by Philipp and Taft[17] found some inconsistencies in their results indicating that the experimental reflectance values were too low, at least for energies greater than 16 eV.

The previously mentioned changes in the 7 eV peak at low temperature seen by CDH were interpreted by Phillips[18] as due to a hybrid exciton at the Γ point. Consistent with this view he considered the drop in low temperature reflectance as the start of an antiresonance and assumed the low temperature curve would display a minimum and rejoin the room temperature value near 8.3 eV. On this basis he placed the direct interband edge $\Gamma_{25'} \rightarrow \Gamma_{15}$ at 8.7 eV rather than near 7 eV as proposed by previous work.

Recently a theoretical discussion by Duke and Segall[19] suggested the nonexistence of hyperbolic excitons. Since the hybrid exciton model proposed for the 7 eV peak in diamond by Phillips uses the hyperbolic exciton as a basis, this new result casts doubt on Phillips' interpretation.

In reply to Duke and Segall[19], Hermanson[20] has reaffirmed the existence of hyperbolic excitons. Thus at this time the existence of hyperbolic excitons is still an open question.

Correlation of experimentally determined optical spectra of solids with the theoretical calculations is obtained by means of the optical constants. Only recently[2] has there been a theoretical interpretation available for explaining the optical constants associated with ultraviolet electronic states in solids.

The optical constants of a solid are defined by the electromagnetic field equations in the following way. The wave equation for the electric field in a conducting medium in MKS units is

$$\nabla^2 \vec{E} - \sigma\mu \frac{\partial \vec{E}}{\partial t} - \varepsilon\mu \frac{\partial^2 \vec{E}}{\partial t^2} = 0. \qquad (2)$$

When the conductivity is zero ($\sigma = 0$) the familiar plane wave solution in terms of the index of refraction n can be written

$$\vec{E} = \vec{E}_o \, e^{i\omega(\frac{nz}{c} - t)} \tag{3}$$

where $n^2 = \varepsilon\mu$. This solution represents a wave traveling in the z direction with velocity $v = c/n$. The case of finite conductivity ($\sigma \neq 0$) suggests a solution of similar form

$$\vec{E} = \vec{E}_o \, e^{i\omega(\frac{Nz}{c} - t)} \tag{4}$$

which is a solution if

$$N^2 = \varepsilon\mu + \frac{i\sigma\mu}{\omega} . \tag{5}$$

N is the complex index of refraction and defined by

$$N = n + ik \tag{6}$$

where k is the extinction coefficient. Thus Eq. 4 can be written

$$\vec{E} = \vec{E}_o \, e^{i\omega(\frac{nz}{c} - t)} \; e^{-\frac{\omega k z}{c}} \tag{7}$$

which represents a damped traveling wave. A complex dielectric response function $\hat{\varepsilon}$ can also be defined

$$\hat{\varepsilon} = \varepsilon\mu + \frac{i\sigma\mu}{\omega} = \varepsilon_1 + i\,\varepsilon_2 \tag{8}$$

from which

$$N^2 = (n^2 - k^2) + i2nk = \hat{\varepsilon} = \varepsilon_1 + i\,\varepsilon_2. \tag{9}$$

It then follows by equating real and imaginary parts that

$$\varepsilon_1 = n^2 - k^2 \tag{10}$$

$$\varepsilon_2 = 2nk.$$

From a theoretical point of view ε_2 is the most important parameter.

In order to obtain the optical constants (n,k) in terms of reflection measurements, consider a monochromatic plane wave (E,H) incident upon the interface between a vacuum and an absorbing medium giving rise to reflected (E',H") and refracted (E",H") waves. The absorbing medium is assumed to be both homogeneous and isotropic. This situation is shown in Figure 2.

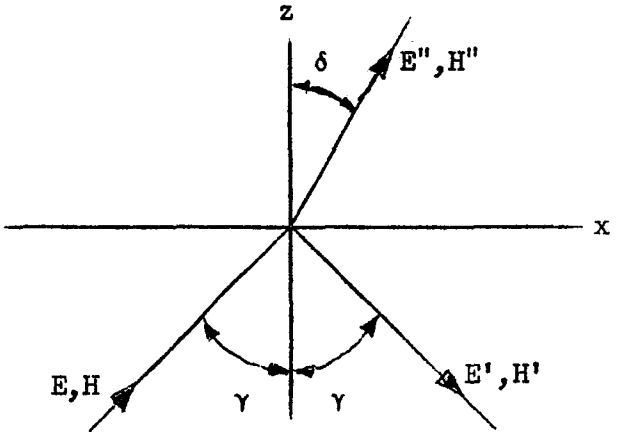

Fig. 2. Electromagnetic field relations at the interface of two media.

For normal incidence, which is pertinent to this research, the angles γ and δ are zero and the direction of the electric and magnetic vectors is meaningless. Using two of Maxwell's equations

$$\nabla \times \vec{E} = - \frac{\partial \vec{B}}{\partial t} \qquad (11)$$

$$\nabla \times \vec{H} = - \vec{J} + \frac{\partial \vec{D}}{\partial t}$$

and the boundary conditions that the tangential components of $\vec{E}$ and $\vec{H}$ are continuous, the ratio $\hat{r}$ of the reflected to incident amplitude is[21]

$$\frac{E'}{E} = \frac{n + ik - 1}{n + ik + 1} = \hat{r} \tag{12}$$

with a similar result for H'/H.

The relfected power or reflectance R is

$$R = \hat{r}\hat{r}^* = r^2 \qquad r = |\hat{r}|. \tag{13}$$

The complex reflection amplitude $\hat{r}$ can be written

$$\hat{r} = \frac{n + ik - 1}{n + ik + 1} = re^{i\theta} = r(\cos\theta + i \sin\theta) \tag{14}$$

where θ is the angle of phase change between the incident and reflected electric field amplitudes. Equating the real and imaginary parts give two simultaneous equations

$$\begin{aligned} k \sin\theta + (n + 1) \cos\theta &= \frac{n - 1}{r} \\ k \cos\theta - (n + 1) \sin\theta &= k/r. \end{aligned} \tag{15}$$

The four inter-related parameters (r, θ, n, k) imply that knowledge of any two determines the remaining pair, for example

$$\begin{aligned} n &= \frac{1 - r^2}{1 + r^2 - 2r \cos\theta} \\ k &= \frac{-2r \sin\theta}{1 + r^2 - 2r \cos\theta}. \end{aligned} \tag{16}$$

From Eq. 10, ϵ_1 and ϵ_2 can be determined in terms of (r,θ). The expression for ϵ_2 is

$$\epsilon_2 = -\frac{4r(1 - r^2) \sin\theta}{(1 + r^2 - 2r \cos\theta)^2}. \tag{17}$$

Since r can be found from a reflectance experiment ($r = \sqrt{R}$, where R is the measured reflectance), the evaluation of n, k, ε_1, and ε_2 depend on a determination of the phase angle θ.

The electronic states of a solid on the one-electron band model are usually depicted by an energy (E) versus crystal momentum ($\vec{k}$) diagram for various directions in $\vec{k}$ space. On these diagrams we can also indicate the basic electronic excitations, e.g., direct and indirect transitions and excitons. For direct or vertical transitions the final electronic state $\vec{k}$ value is the same as that of the initial state in contrast to indirect transitions where the initial and final electron state $\vec{k}$ values are different. According to the Bloch model of solids $\vec{k}$ is conserved and thus indirect transitions involve interactions with other excitations such as phonons.

It is possible to distinguish experimentally between these elementary excitations, e.g., the absorption coefficient for direct transitions is of the order of 10^5 to 10^6 cm^{-1} while that for indirect transitions is of the order of 10^3 cm^{-1}. Similarly the temperature dependence of excitons differs from that of both direct and indirect transitions.

The theoretical expression for ε_2,[22] for direct transitions where lifetime broadening has been neglected, is

$$\varepsilon_2(\omega) = \frac{e^2h^2}{m} \sum_{i,j} \frac{1}{\Omega} \int \frac{f_{ij}(\vec{k})}{E_{ij}|\nabla_k E_{ij}|} \, dS_k \qquad (18)$$

where $E = \hbar\omega$ and the integral is over a surface of constant energy, $E_{ij}(\vec{k}) = E_j(\vec{k}) - E_i(\vec{k})$. In this expression Ω is the volume of the first Brillouin zone, the letters i and j denote valence and conduction band states respectively and f_{ij} is the electronic oscillator strength. The density of states having the energy differences E_{ij} is proportional to

$$\frac{dN}{dE_{ij}} \sim \int \frac{dS_k}{|\nabla_k (E_j - E_i)|} . \tag{19}$$

We see that the line shape of ε_2 is determined primarily by f_{ij} and $\nabla_k E_{ij}$. Phillips[22] has shown that for ionic crystals where the electrons are tightly bound the oscillator strength, f_{ij}, is approximately constant throughout the Brillouin zone and thus $\nabla_k E_{ij}$ determines the line shape for these materials. For normal metals where the electrons are more nearly free the situation is much different and the variations in f_{ij} become quite important. To the extent that arguments based on a tight binding model can be applied to covalent materials such as diamond we will assume that the structure in ε_2 for diamond is determined by $\nabla_k E_{ij}$. Thus we consider bands i and j for which f_{ij} is nearly constant throughout the Brillouin zone and replace f_{ij} by $\overline{f_{ij}}$. With this approximation ε_2 is proportional to the interband density of states given by

$$\frac{dN}{dE_{ij}} = \Omega^{-1} \int \frac{dS_k}{|\nabla_k (E_j - E_i)|} . \tag{20}$$

The behavior of $\epsilon_2(\omega)$ or $\frac{dN}{dE_{ij}}$ is singular at those points in $\vec{k}$ space called critical points for which

$$\nabla_k E_{ij}(\vec{k}) = \nabla_k E_j(\vec{k}) - \nabla_k E_i(\vec{k}) = 0. \tag{21}$$

This can occur at various points on the surface $\hbar\omega = E_j - E_i$.

Van Hove[23] was the first to point out the significance of such critical points. Phillips[24] has shown that the number of such points can be restricted by considerations of symmetry and connectivity. Phillips[22] also distinguishes between symmetry interband points (s.i.p.) for which

$$(\text{s.i.p.})\ \nabla_k E_j(\vec{k}) = \nabla_k E_i(\vec{k}) = 0 \tag{22}$$

and general interband points (g.i.p.),

$$(\text{g.i.p.})\ \nabla_k E_j(\vec{k}) = \nabla_k E_i(\vec{k}) \neq 0. \tag{23}$$

The s.i.p.'s occur only at points of high symmetry in the Brillouin zone such as $\vec{k} = 0$ whereas the g.i.p.'s may occur on symmetry lines, planes or general points; i.e., whenever the slopes are equal.

The analytical behavior of the joint density of states function near a critical point may be obtained by a Taylor series expansion of $E_j(\vec{k}) - E_i(\vec{k})$ about the critical point $\vec{k}_o$.

$$E_j(\vec{k}) - E_i(\vec{k}) = \hbar\omega_o(\vec{k}_o) + \sum_{i=1}^{3} a_i (k_i - k_{oi})^2. \tag{24}$$

When all the coefficients a_i are positive (negative) we have a minimum (maximum) in the interband joint density of states and this situation is denoted M_o (M_3). Mixed signs of the a_i correspond to saddle points and are denoted M_1 and M_2. When the above expression is substituted

into the expression for the interband joint density of states relation we find; e.g., near an M_1 singularity

$$\begin{aligned} \frac{dN}{d\omega} &= C_1 - C_2 (\omega_o - \omega)^{1/2} && \omega \leq \omega_o \\ &= C_1 && \omega \geq \omega_o \end{aligned} \tag{25}$$

where C_1 and C_2 are constants. The general shape of an M_o edge as well as the other types is shown in Figure 2(a), (b), (c), (d). As Phillips[22] points out "the most important qualitative aspect of Van Hove singularities is that a simple singularity does not produce a peak but only an edge. To obtain a narrow plateau or "peak", M_1 and M_2 singularities must be almost degenerate." This condition for a peak is indicated in Figure 2(e).

The preceding discussion indicates why the structure in ε_2 is important. A shoulder has a different theoretical interpretation than a peak and thus accurate experimental results are necessary.

Consider how this general interpretation of optical constants in terms of the density of states and critical points applies to diamond in particular. The crystal structure and first Brillouin zone of diamond are shown in Figure 4. This structure corresponds to two interpenetrating face centered cubic lattices while the 1st zone is a truncated octahedron. The principal lines and points of symmetry are indicated; e.g., Γ denotes the center of the zone and L the midpoint of the hexagonal face.

In the preceding section we indicated that at points of high symmetry such as Γ, X and L, the gradients of the energy functions for

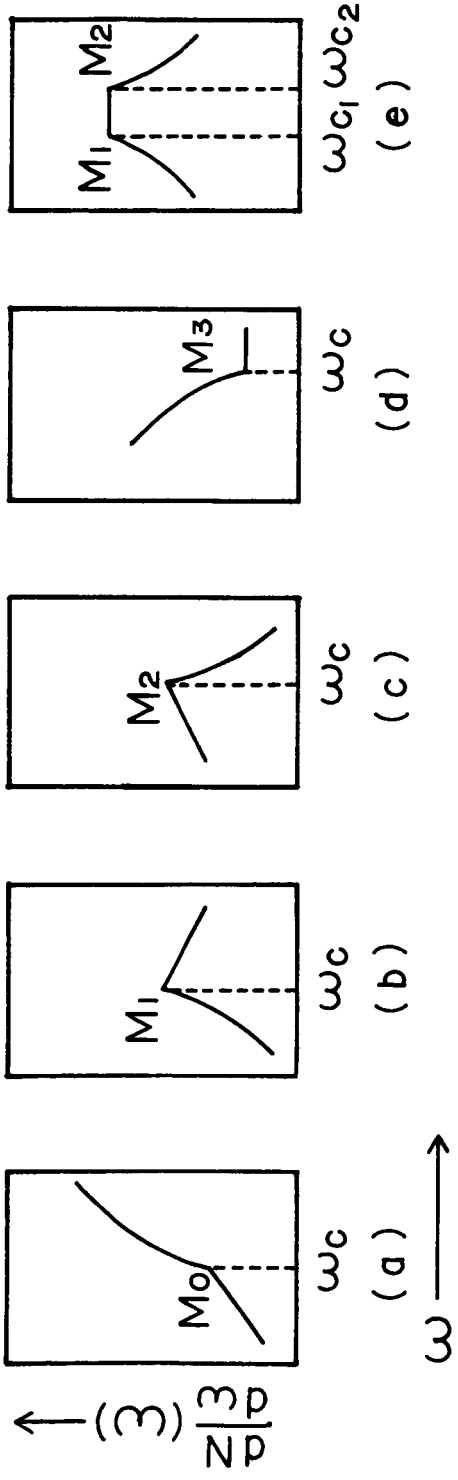

Fig. 3. Types of singularities in the electronic interband density of states.

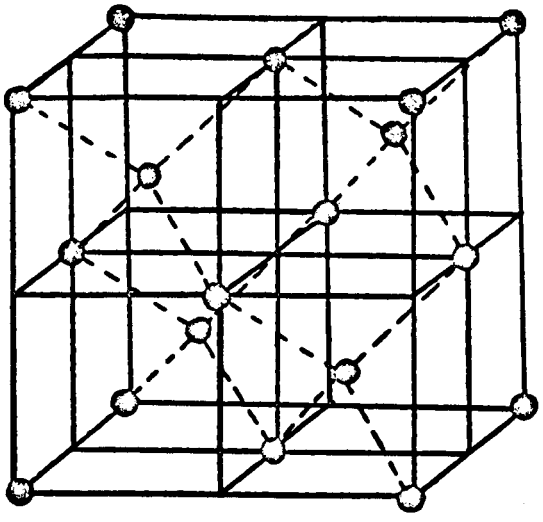

DIAMOND STRUCTURE

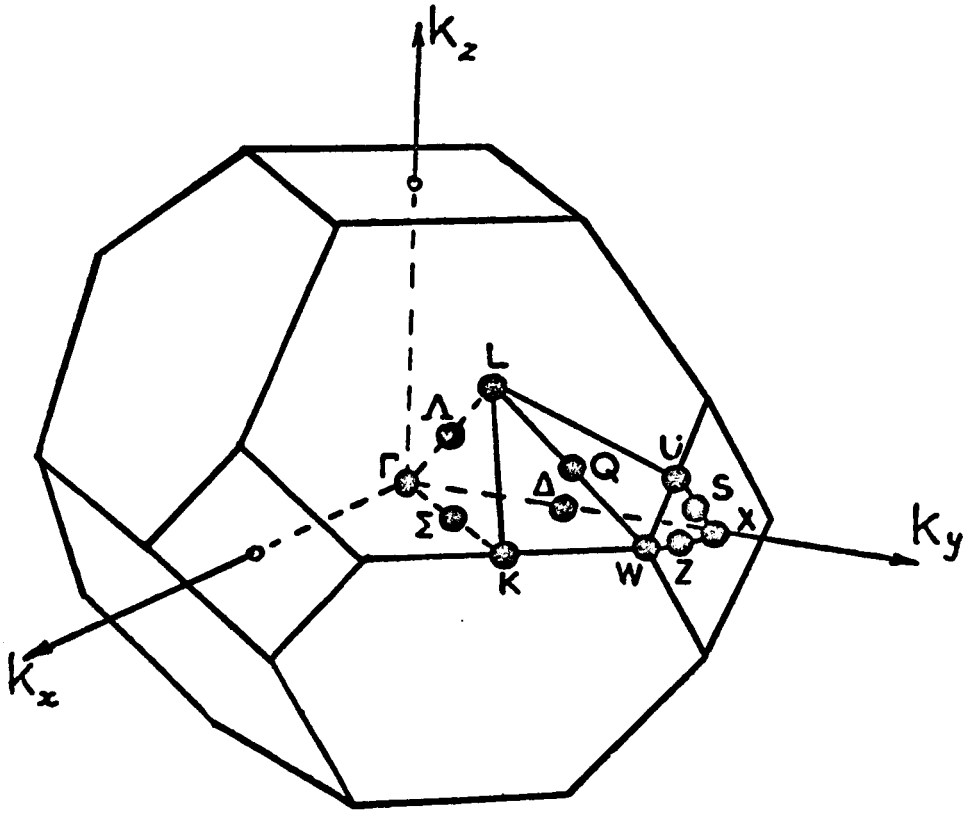

BRILLOUIN ZONE

Fig. 4. The crystal structure and first Brillouin zone of diamond.

the conduction and valence bands vanish, thus giving rise to singularities in the joint density of states function. Since ϵ_2 is proportional to the joint density of states function we expect to see structure in ϵ_2 corresponding to these singularities.

Figure 1 compares two recent band calculations for diamond. Some of the points and lines of high symmetry corresponding to those of the Brillouin zone are indicated. By a brief perusal of the band structure we might expect to find structure in ϵ_2 at Γ, X, L since the conditions for singularities in the joint density of states exists at these points.

From Figure 1 we see that the indirect edge or onset of indirect transitions occur from $\Gamma_{25} \rightarrow \Delta_1$ where Δ_1 is a point about three quarters along the [1,0,0] direction. This transition corresponds to an energy of 5.47 eV as determined by Dean et al.[25]

The direct edge or onset of direct transitions occurs from $\Gamma_{25} \rightarrow \Gamma_{15'}$. This corresponds to an energy near 7 eV with some variation between the two calculations.

In the chapter on Results and Discussion we will consider detailed interpretation of this and other points.

III. EXPERIMENTAL DETAILS

Absolute reflection spectra at near normal incidence were obtained in the present research in the range 5.5 - 31 eV at both 300 and 77°K with a system composed of a McPherson 225 monochromator, various ultraviolet sources, a specially constructed low temperature reflectometer and associated recording equipment. A schematic view of the optical system is shown in Figure 5.

A McPherson Model 225 one meter normal incidence scanning monochromator was used with a 1200 line/mm grating blazed at 1500 Å giving a first order dispersion of 8.3 Å/mm. The grating was magnesium fluoride coated to increase its efficiency in the vacuum ultraviolet. The monochromator was evacuated by an oil diffusion pump and as an independent unit could maintain a vacuum slightly better than 1×10^{-6} torr. The wavelengths of the source lines could be read directly from a mechanical counter to an accuracy of 1 Angstrom.

For the work above 1100 Å a hydrogen glow discharge was used. Figure 6 (a) shows a photograph of the lamp. The main body or electrodes of the light source was made entirely of copper and brass. An earlier model of the source was made of aluminum but it was found that the cooling tap water, filtered through a water softener, reacted with the aluminum and caused white deposits to build up rapidly. No short term deposit problem was apparent with the brass and copper construction. As indicated in Figure 6 (a) both the anode and cathode were cooled by circulating cold water.

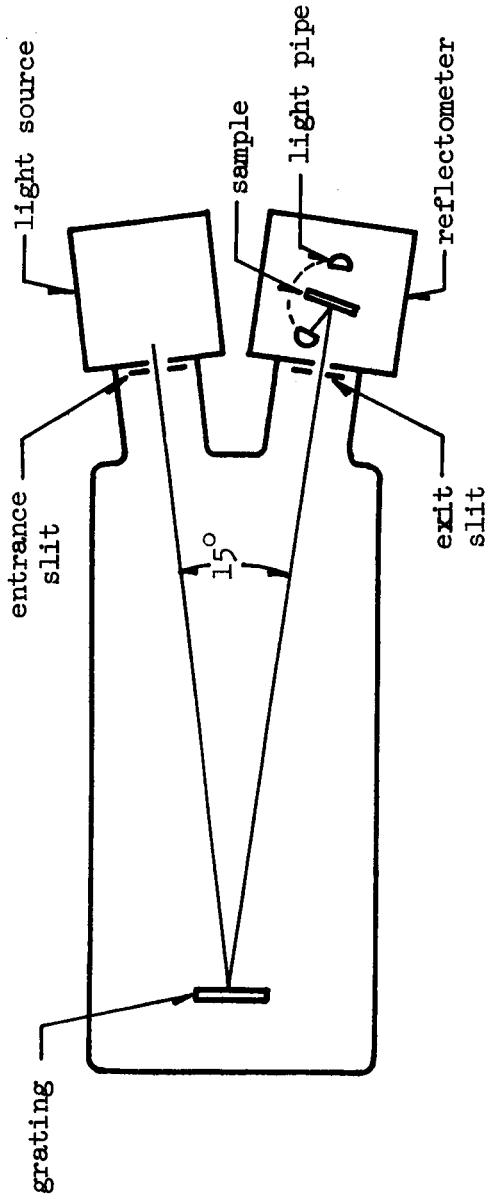

Fig. 5. Diagram of the optical system.

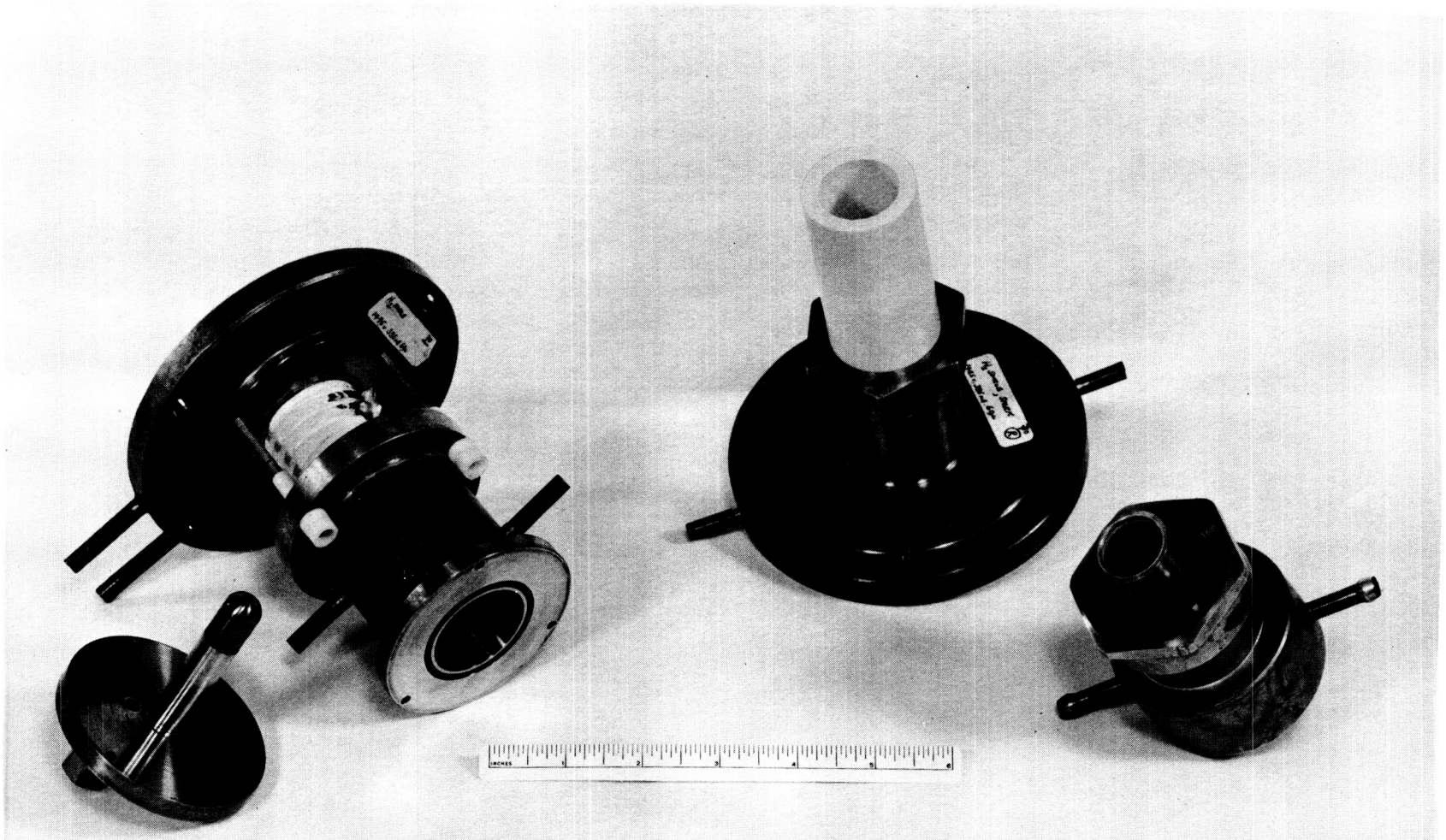

Fig. 6. Ultraviolet light sources (a) hydrogen glow (b) argon pulse.

Boron nitride was used to contain the discharge in a one-eighth inch diameter capillary. O-ring finishes and cooling fins were easily machined in the boron nitride. A fan provides additional cooling for the source by blowing cool air through the finned surfaces. The boron nitride electrically separated the anode from the cathode and insulated screws mechanically coupled these electrodes in position. A copper-tungsten alloy was used on the tip of the cathode because of the low high voltage sputtering quality of this material. A small hole in the tip allowed visual inspection of the discharge through a window on the rear of the cathode.

This source was powered by a Kepco Model HB 2050 power supply capable of 2000 volts at 500 milliamps. This supply was voltage regulated. However, it was found that a current regulated supply would be more desirable for maintaining constant line intensities. A load resistor between the power supply and the lamp prevented avalanching of the source current.

The gas discharge was stable over a large range of gas pressure but normal operating conditions using 300 micron entrance and exit slits showed a source pressure of 10 microns with 4×10^{-5} torr in the main chamber of the monochromator. For these conditions the power supply was operated at 1400 volts and 400 milliamps, 500 volts of which were dropped across the lamp giving 250 watts of power dissipated in the source.

Below 1100 Å, argon gas was used in the lamp shown in Figure 6 (b). This lamp was similar to the hydrogen lamp but modified by replacing the

insulating screws holding the electrodes together by electrodes which independently gripped the boron nitride. This change was necessary because of the higher voltages involved in this discharge.

The lamp was excited by a pulsed power supply made from a modified thyratron tube testing unit giving approximately 40 pulses per second to the light source during normal operation. A simple diagram of the high voltage pulse power supply is shown in Figure 7. Excited in this manner, a useful line spectrum was obtained extending from Lyman α (1216 Å) down to 350 Å.

Excitation of the light source occurs as follows. The 1200 volt power supply charges capacitor C_1 through resistor R_1, coil L and the igniter-rod circuit. At the same time the main power supply charges capacitor C_2 through the resistors R_2 and R_3. When the thyratron grid potential is adjusted by the triggering unit to permit conduction, the capacitor C_1 charge will pass through the thyratron and igniter-rod circuits. The ignitron will conduct provided the ignitron anode potential is sufficiently positive to maintain the discharge voltage potential existing across C_2 to the light source which in turn will cause ionization of the gas and a subsequent capacitor discharge through the lamp giving rise to radiation from multiple ionized atoms. The current surge through the igniter-rod circuit will quickly discharge the capacitor C_1, the thyratron anode potential will fall below that needed to maintain the arc in the thyratron, the thyratron igniter-rod circuit current will fall to zero and the ignitron will fail to

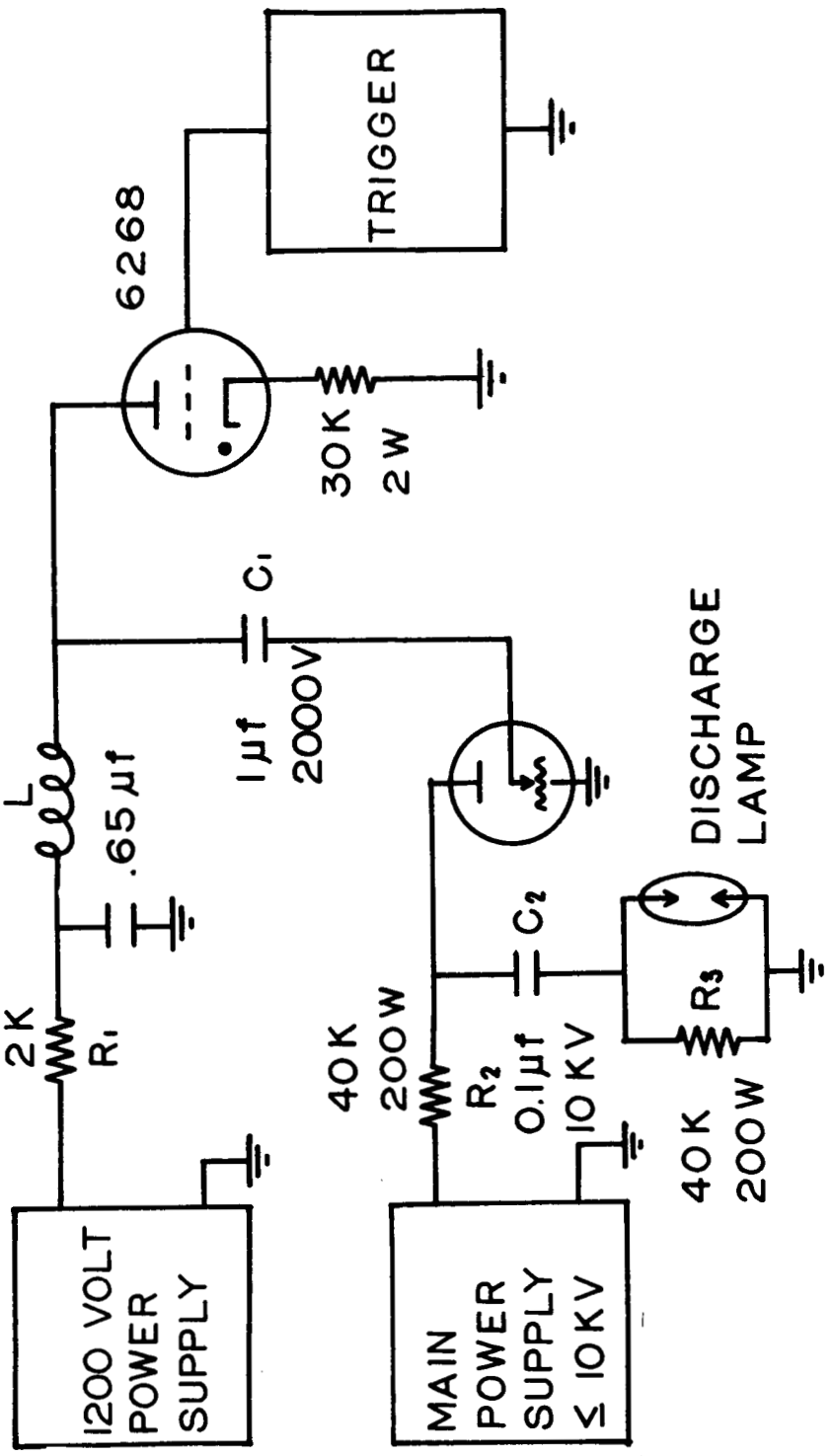

Fig. 7. Schematic diagram of the high voltage pulse power supply.

conduct thus quenching the light source. The capacitors C_1 and C_2 will then be recharged in time for the next cycle.

Using the hydrogen gas source, data points were obtained with relative accuracy of 1% whereas with the argon source there was a 5% scatter of points. Thus the high energy results between 13 and 19 eV should be considered less reliable than results at lower or higher energies.

The low temperature reflectometer was constructed of stainless steel with viton O-rings seals where necessary. The reflectometer was cylindrical in shape with four ports at right angles as shown in Figure 8.

A leak valve for bringing the reflectometer chamber up to atmospheric pressure was mounted on one port. Through the same port the thermocouple wires for monitoring the sample temperature were brought out through a kovar seal and sealed with high vacuum epoxy to the feed throughs. Inside the reflectometer a copper-constantan thermocouple junction was attached to the sample holder.

The top port contained the mechanism for positioning the sample by rotation or up and down motion. Attached to this mechanism was the sample holder itself which consisted of a one inch diameter stainless steel tube approximately 16 inches long with a cylindrical copper block welded on the bottom end. Figure 9 shows the details of the sample holder. Samples were mounted on a $\frac{1}{4}$" x $\frac{1}{2}$" x 1" copper block with a small amount of epoxy and the copper block was fastened with two Allen head screws to a $\frac{1}{2}$" slot in the sample holder. With the sample block

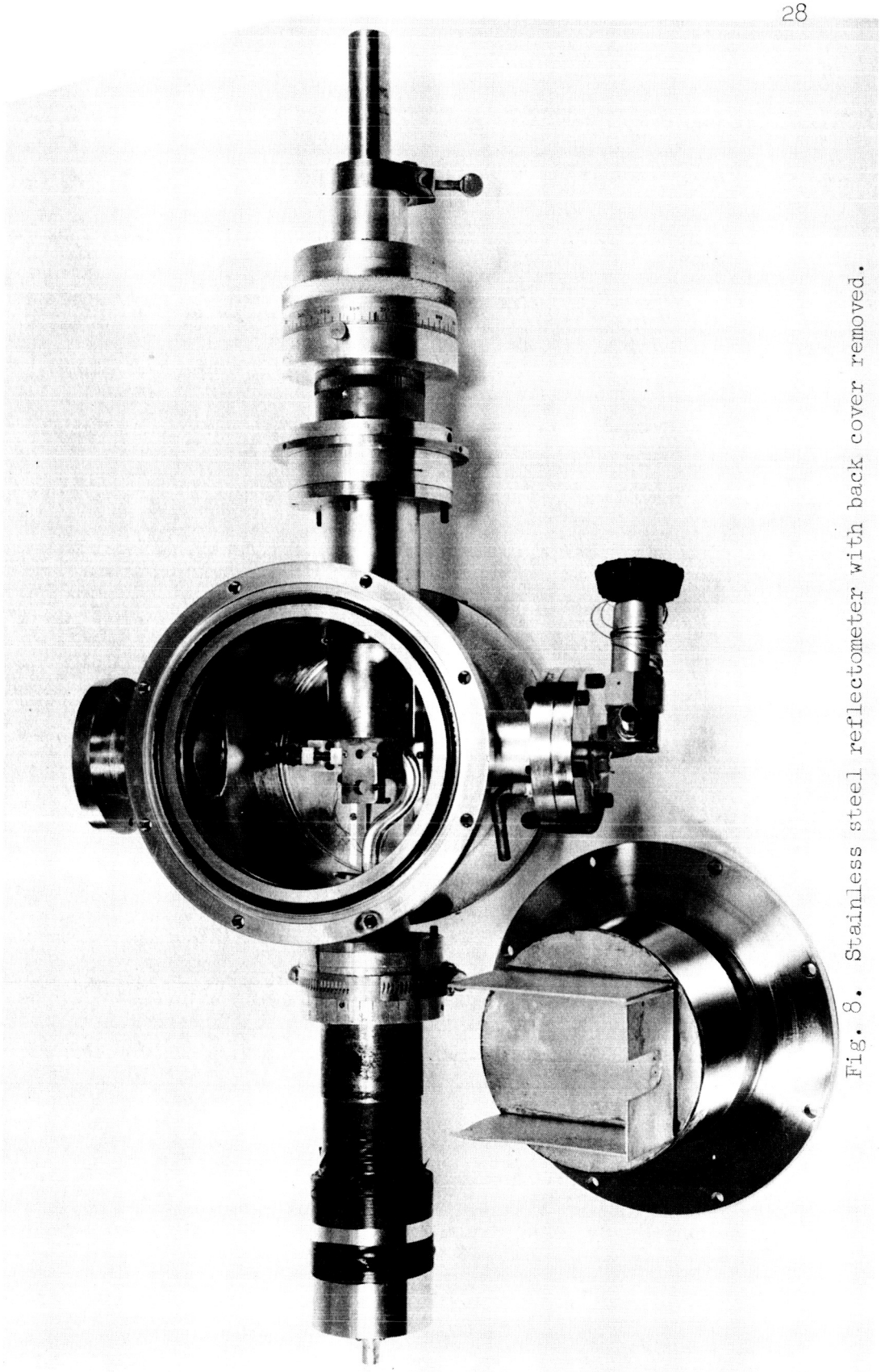

Fig. 8. Stainless steel reflectometer with back cover removed.

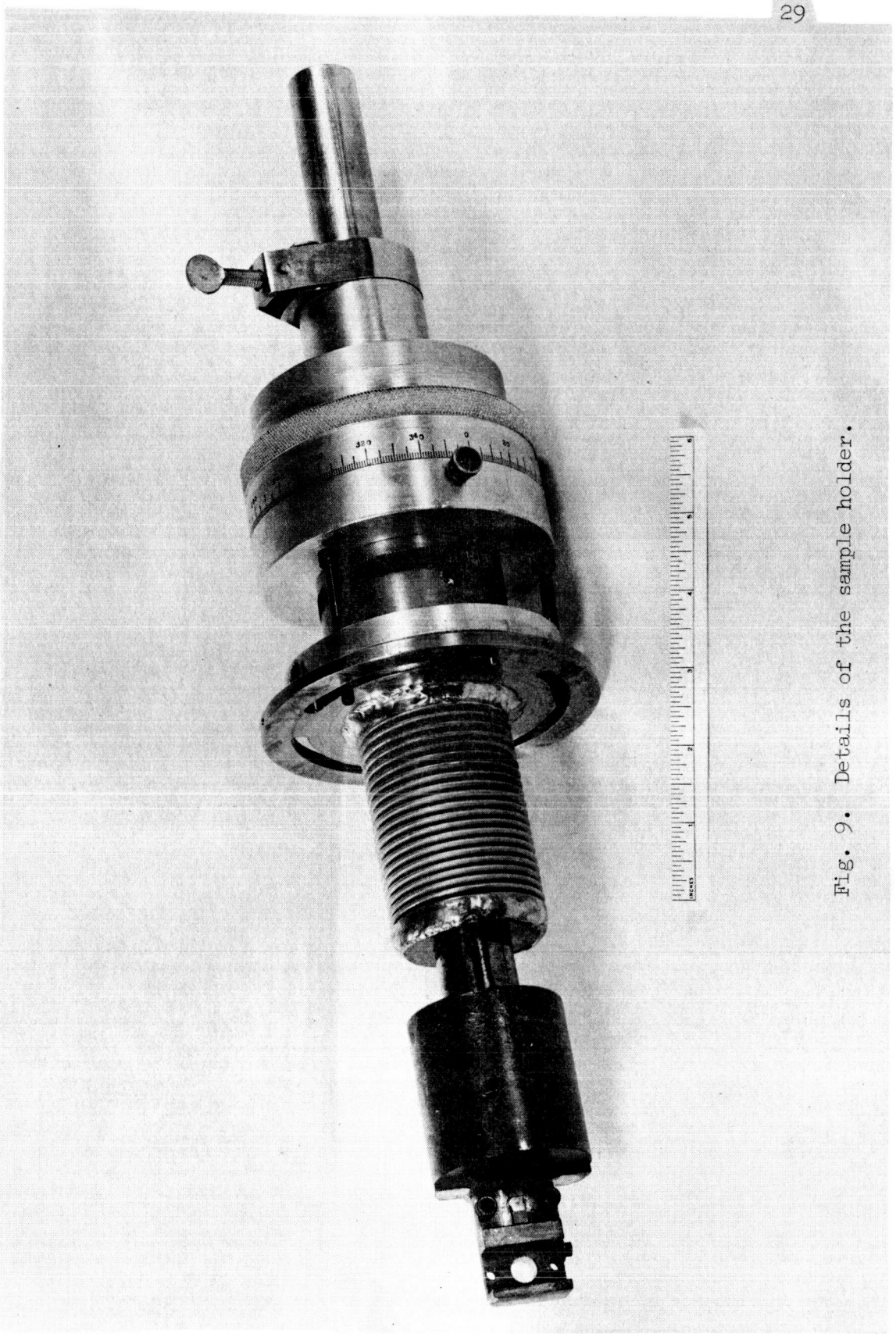

Fig. 9. Details of the sample holder.

in position in the sample holder it was then possible to cool or bake the sample by putting either liquid nitrogen on a heating tape down the stainless steel tube of the sample holder. The reflectometer and sample holder were designed so that the face of the sample pivoted around the tube axis upon rotation of the sample holder.

A stainless steel bellows was welded around the stainless steel tube of the sample holder so that vertical motion could be transmitted without breaking the vacuum seal. In the early stages of experimentation no bellows was used and vertical motion was obtained by sliding the tube through a double teflon O-ring seal. The method was found to be inadequate as vertical motion would introduce a small vacuum leak. In the final design with bellows the double O-rings were utilized for axial alignment of the sample holder tube and provided no vacuum seal.

The vertical motion device was made from aluminum using ball bearing in the rotating parts. An externally threaded collar rigidly clamped to the sample holder tube provided the vertical motion when a larger internally threaded collar was turned. This outer collar was fixed in vertical position but rotatable so that when turned the action of the threads transfered vertical motion to the tube. This mechanism in conjunction with the bellows gave approximately one inch of vertical travel.

Rotary motion of the sample was accomplished in the following manner. On the upper end of the bellows a flange was welded which in turn was O-ring sealed to the reflectometer body and held in position by three screws. The flange was slotted and allowed rotation of nearly

90° with the screws in position. When it was desired to rotate the sample the three screws were loosened and the sample holder rotated by turning the flange. This operation could be performed with the reflectometer under vacuum although rotation did cause slight air leakage. The leakage did not cause any problem since it was not found necessary to change the angle of rotation during the reflection run. Instead the desired angle of rotation was selected and fixed prior to initiation of the measurement.

The bottom port of the reflectometer contained a sodium salicylate coated pyrex light pipe in the shape of a question mark which could be rotated to monitor either the incident or reflected beam. An EMI 6256 photomultiplier tube was positioned at the bottom of the light pipe. This tube has its peak efficiency near the peak of the fluorescence from the sodium salicylate, namely 4400 Å. The photomultiplier was powered by a John Fluke, D.C. Power Supply and normally operated at 1050 volts. Signal output from the photomultiplier was fed into a Keithley Model 417 picoammeter. The output of the picoammeter which ranged from 0 to 3 volts on all scales was then fed through a potentiometer network to a 10 millivolt Leeds & Northrup strip chart recorder.

The remaining reflectometer side port was used during low temperature measurements for evacuating the reflectometer separately from the monochromator. For low temperature work a lithium fluoride window was used as a vacuum seal between the monochromator and the reflectometer systems. A Varian 15 liter/sec. Vacion-titanium sublimation pumping

system attached to the port was able to maintain the reflectometer chamber at a pressure of better than 10^{-7} torr. This separate pumping system guaranteed that the sample in the reflectometer was not exposed to oil vapors from the diffusion pump of the monochromator. The Vacion pump operates on a different principle than diffusion pumps, namely the gas atoms in the reflectometer are ionized and then react with the titanium surface in the pump forming stable compounds. Because sample surface is a severe problem in reflection measurements obtaining a clean environment at low temperature involved a major experimental effort. During room temperature measurements the port was sealed off and the window between the reflectometer and monochromator removed.

The back plate of the reflectometer was removable and had attached to it a cylindrical copper reservoir with protruding fins. The copper fins extended to surround the sample holder from the sides and bottom. When the reservoir was filled with liquid nitrogen the fins served as a cold shield to trap any condensable molecules remaining in the reflectometer which might have settled on the cold sample surface.

The low temperature experimental procedure is described below. The room temperature procedure is the same except the sample is not cooled and the window and Vacion pumping system are removed.

With the window in place the light source was first turned on to stabilize before preparation of the sample was begun. A sample was then mounted to the small copper block and given an acetone scrub and methanol rinse to remove any possible oil contamination on the crystal

surface. The evaporating methanol was visually observed to be sure that drops of fluid not shaken off did not remain on that part of the crystal to be illuminated by the incident beam. An additional aperature was placed in the reflectometer to ensure that the area of the incident beam striking the crystal was smaller than the crystal surface area itself.

With the sample now ready for placement in the reflectometer, the reflectometer chamber was quickly brought up to atmospheric pressure and the back plate removed. A visual check was made to see if the hole in one of the slots in the sample holder aligned with the exit slit aperatures.

The sample mounting block was next inserted into the alternate slot of the sample holder and secured by two screws. Then the sample holder was rotated until it appeared that the sample surface was nearly perpendicular to the direction of the incident beam. The light pipe was turned into position for measuring the incident beam. After the back plate of the reflectometer was replaced, the reflectometer was evacuated by first rough pumping with a liquid nitrogen cooled sorption pump and then further evacuated by the Vacion pump. Total time from cleaning to a vacuum of about 10^{-6} torr was approximately 6 minutes.

As soon as the back plate was in place the photomultiplier high voltage was applied in order to allow the dark current to reach a steady value. Having previously adjusted the sample holder so that the incident beam was coming through the open hole, the light pipe was

adjusted to obtain a maximum signal. The sample holder was then rotated until the decreasing effective area of the hole began to cut off the beam reaching the light pipe with a resultant drop in signal. At this point the sample holder was fixed in position by the three screws holding it to the body of the reflectometer. For the particular hold size used this angle of rotation was about 11° from normal incidence which was conveniently close enough to the assumption of normal incidence used in the experimental interpretation. Using an angle larger than 11° would have resulted in relative instead of absolute reflection data since part of the reference beam would have been lost. The smallest limiting angle was about 4° off normal at which point the light pipe when rotated to pick up the reflected beam would begin to interfere with the incident beam.

The sample was then moved into the incident beam by means of the vertical motion device. Thirty complete turns of the screw mechanism corresponded to the distance between the two sample holder hole centers. The light pipe was then rotated into position for measuring the beam reflected from the sample surface. This position was optimized by observing the maximum signal from the photomultiplier. To insure that the incident beam was entirely on the surface of the crystal the sample holder was raised and lowered until the maximum signal was obtained.

With the crystal now in the optimum position for measurement so that no further rotation would be necessary the reflectometer and sample were baked overnight at approximately 140°C. which helped to drive off

any water vapor present. Baking temperatures higher than this were avoided because of the epoxy and O-ring seals present. The sample heating was accomplished by placing a heating tape in the stainless steel tube of the sample holder. The sample temperature was monitored and adjusted by varying the current through the heating tape.

After the overnight sample bake was completed the heating tapes were removed and the light source turned on to stabilize while further preparations were continued. When the reflectometer had cooled sufficiently, liquid nitrogen was added to the rear flange reservoir approximately thirty minutes before the sample itself was to be cooled. This allowed any condensable molecules not removed by baking to freeze out on the large cold surface area of the reservoir rather than on the cold sample surface.

While monitoring the reflected beam the sample was next cooled by pouring liquid nitrogen down the stainless steel tube of the sample holder. The copper block on the end of the tube was in thermal contact with the sample mounting block itself and thus the sample was cooled by conduction. If any continuous decrease in reflection was observed after the sample was cooled it was taken as an indication of impurities building up on the cold sample surface. Such reflectance drop was noticed at two stages of the experiment. Firstly, in the original reflectometer design a sliding device having several interchangeable windows with different transmission characteristics was used. An O-ring was used to isolate this mechanism from the monochromator but

still enough leakage, possibly oil vapor, from the monochromator caused a reflectance drop. Secondly, before the bellows was attached to the sample holder vertical motion caused very small pressure increase but quite striking reflectance loss.

With the monitoring precaution observed and no reflectance decrease the reflection spectrum over the region of interest was then taken. The sample was next moved out of the beam, the light pipe rotated and a measurement of the incident beam intensity taken. Another reflection measurement followed by an additional incident measurement completed the run giving two separate measurements to average.

IV. DATA ANALYSIS

A. KRAMERS-KRONIG RELATIONS

When the absorption coefficient is extremely high, transmission measurements can no longer be made to determine the optical properties of solids. Recently, attention has turned to reflection measurements using Kramers-Kronig analysis for determination of these properties. Reflection measurements at near normal incidence offer considerable advantages over those made well away from normal incidence. These advantages include simpler theoretical expressions and insensitivity of most materials to polarization effects at small angles. At the same time however the simpler expressions mean that we have only a single reflectance relation of the form $R(n,k)$ and thus do not have sufficient information to determine n, k independently. However there is one more relationship which can be invoked through the use of dispersion relations.

Dispersion relations in general express the interdependence of the real and imaginary parts of complex functions satisfying certain conditions. For example consider the complex function $\hat{F}(\omega) = Q(\omega) + i\,P(\omega)$, the dispersion relation between P and Q is

$$P(\omega_o) = \frac{1}{\pi} \int_o^\infty \ln \frac{\omega + \omega_o}{\omega - \omega_o} \frac{d\,Q\,(\omega)}{d\omega} \, d\omega. \qquad (26)$$

In optics it has been shown that such relations may be applied to the complex refractice index, the complex dielectric function and the complex reflection amplitude.

The optical constant of theoretical interest is the imaginary part of the complex dielectric response function. From the Fresnel equations for normal incidence (reflectivity $r = |\hat{r}|$, $R = \hat{r}\hat{r}^* = r^2$) the imaginary part of the dielectric function can be written

$$\varepsilon_2 = - \frac{4r(1 - r^2) \sin \theta}{(1 + r^2 - 2 r \cos \theta)^2} \tag{27}$$

where θ is the angle of phase change of the electric field upon reflection. The angle θ can be determined from the reflectance spectrum by an integral transformation or dispersion relation first employed by Kramers and Kronig. This relation states that the phase angle θ for any frequency ω_o is given by

$$\theta(\omega_o) = \frac{1}{\pi} \int_o^\infty \ln \left| \frac{\omega + \omega_o}{\omega - \omega_o} \right| \frac{d \ln r(\omega)}{d\omega} \, d\omega. \tag{28}$$

Thus, by determining θ from a knowledge of R we can then obtain ε_2, in fact knowledge of r, θ means we can determine ε_1, ε_2, n, and k since any constant can be expressed in terms of any other two, i.e., $n(r,\theta)$, $k(r,\theta)$, $\varepsilon_1(r,\theta)$, $\varepsilon_2(r,\theta)$.

The difficulty in applying this relation is that the whole of the electromagnetic spectrum contribues to the value of the angle at any particular frequency ω_o. First it is noticed from Eq. 28 that it is not the reflectance spectrum but the derivative of its logarithm with respect to frequency which contributes to the phase angle. Thus regions in which the reflectance is changing slowly with frequency contribute very little to the phase angle. The weighting function $\ln \left| \frac{\omega + \omega_o}{\omega - \omega_o} \right|$ is largest near $\omega = \omega_o$ and decreases rapidly as the difference

$\omega - \omega_o$ increases. Thus while the phase angle θ evaluated at ω_o depends on the entire frequency range, in fact only the frequency range in the neighborhood of ω_o contributes significantly. The contribution from the low frequency side can be easily included by simple extrapolation of the reflection data using known values of the index of refraction in transparent regions. In general however the high frequency side is characterized by intense continuous absorption and no generally applicable technique is available for determining the high frequency contribution. The usual method has been to assume a somewhat arbitrary smooth extrapolation of experimental data to very high frequencies. Certain assumptions can be made about the behavior of reflectance at very high frequencies but the most sensitive test of any technique is that the phase angle must be zero in regions of no absorption.

An alternate way to treat the high energy contribution developed by Roessler[26] proceeds as follows. In practice the reflectance in some finite region (a,b) is measured. The integral for the phase angle can be written

$$\theta(\omega_o) = -\left[\int_o^a + \int_a^b + \int_b^\infty\right] \tag{29}$$

$$= \alpha(\omega_o) + \phi(\omega_o) + \beta(\omega_o)$$

where the contribution $\phi(\omega_o)$ can be determined from the experimental data. In the interval (0,a), ω is always less than ω_o since ω_o lies in (a,b) and thus $\frac{d}{d\omega} \ln \left|\frac{\omega + \omega_o}{\omega - \omega_o}\right|$ is continuous and positive without

change of sign in (0,a). We can thus apply the generalized mean value theorem for integrals which states that if f(x) and g(x) are continuous functions in $a \leq x \leq b$ and if $g(x) \geq 0$ throughout this interval then

$$\int_a^b f(x)\, g(x)\, dx = f(\zeta) \int_a^b g(x)\, dx \tag{30}$$

where $a \leq \zeta \leq b$. There is only one value of ζ for which this relationship is true. For our situation then we have

$$\begin{aligned} \alpha(\omega_o) &= -\frac{\ln r(\zeta)}{\pi} \int_o^a \frac{d}{d\omega} \ln\left|\frac{\omega + \omega_o}{\omega - \omega_o}\right| d\omega \\ &= A \ln\left|\frac{a + \omega_o}{a - \omega_o}\right| \end{aligned} \tag{31}$$

where $A = -\frac{\ln r(\zeta)}{\pi}$, ζ lying in (0,a) and a similar expression for $\beta(\omega_o)$

$$\beta(\omega_o) = B \ln\left|\frac{b + \omega_o}{b - \omega_o}\right| \tag{32}$$

where $B = \frac{\ln r(\eta)}{\pi}$, η lying in (b,∞).

If one assumes that A,B which are functions of ζ,η respectively, vary only slowly with ω_o (strictly speaking $\zeta = \zeta(\omega_o), \eta = \eta(\omega_o)$) then by choosing two frequencies at which the material in question is known to be transparent (implying $\theta = 0$), A and B can be determined. If for example $\theta = 0$ at $\omega = c, \omega = d$ then

$$\begin{aligned} A \ln\left|\frac{a + c}{a - c}\right| + \phi(c) + B \ln\left|\frac{b + c}{b - c}\right| &= 0 \\ A \ln\left|\frac{a + d}{a - d}\right| + \phi(d) + B \ln\left|\frac{b + d}{b - d}\right| &= 0 \end{aligned} \tag{33}$$

From these two simultaneous equations A and B may be determined and hence $\theta(\omega_o)$ for all ω_o using Eq. 28 and ϵ_2 from Eq. 27. Any of the other expressions such as n, k, e_1, $-\mathrm{Im}\,\frac{1}{\tilde{\epsilon}}$ can also now be determined.

Let us now consider further the assumption that A and B are nearly independent of ω_o. Roessler[26] has considered this problem by expressing $\alpha(\omega_o)$ in a more general form. This is accomplished by first integrating Eq. 28 by parts to obtain

$$\theta(\omega_o) = -\frac{1}{\pi}\int_o^\infty \ln r(\omega)\,\frac{d}{d\omega}\,\ln\left|\frac{\omega+\omega_o}{\omega-\omega_o}\right|\,d\omega \tag{34}$$

so that

$$\alpha(\omega_o) = -\frac{1}{\pi}\ln\left|\frac{\omega_o+a}{\omega_o-a}\right|\,\ln r(\zeta) \tag{35}$$

where $0 < \zeta < a$.

and a similar expression for $\beta(\omega_o)$

$$\beta(\omega_o) = \frac{1}{\pi}\ln\left|\frac{b+\omega_o}{b-\omega_o}\right|\,\ln r(\eta) \tag{36}$$

where $b < \eta < \infty$.

Now if the frequency dependence of η, ζ can be neglected then we can find A, B and thus evaluate $\theta(\omega_o)$. Note first of all that $\alpha(\omega_o)$ and $\beta(\omega_o)$ are weighed by sharply peaked functions, e.g., $\ln\left|\frac{b+\omega_o}{b-\omega_o}\right|$ which means only when ω_o is close to b will we get a large contribution. The expression for $\alpha(\omega_o)$ can be integrated by parts and written as

$$\alpha(\omega_o) = -\frac{1}{\pi}\ln\left|\frac{\omega_o+a}{\omega_o-a}\right|\left\{\ln r(a) - \int_o^a \frac{\ln[(\omega_o+\omega)/(\omega_o-\omega)]}{\ln[(\omega_o+a)/(\omega_o-a)]}\,\frac{d\ln r(\omega)\,d\omega}{d\omega}\right\} \tag{37}$$

which is exact and general. The expression in curly brackets corresponds to ln r (ζ) and shows its functional dependence on ω_o. We see that there will not be a strong contribution to $\alpha(\omega_o)$ unless ln r (ω) changes rapidly in (0,a) and at the same time ω_o is near a. Thus we expect the bracketed term to be fairly constant except possibly near $\omega_o = a$. A similar argument applies to $\beta(\omega_o)$. In summary then if there is no strong structure outside (a,b) the assumption that A and B are constants is valid. If structure does exist then we must be careful of results obtained near a and b but elsewhere the results are valid. Roessler applied quantitative checks to different materials to show that the errors introduced by this method are much less than the uncertainty in the original reflectance spectrum.

B. COMPUTER TECHNIQUE

The evaluation of the integral transform in the Kramers-Kronig analysis is carried out by computer as follows. The reflectance R is related to n, k and $\hat{r}$ (reflectivity) by the equations

$$R = \frac{(n-1)^2 + k^2}{(n+1)^2 + k^2} \qquad R = \hat{r}.\hat{r}^* \qquad (38)$$

where $\hat{r} = |\hat{r}|\, e^{i\theta}$ $\qquad |\hat{r}| = \sqrt{R} = r$

and $$\hat{r} = \frac{n + ik - 1}{n + ik + 1} = r(\cos\theta + i\sin\theta) \qquad (39)$$

or in terms of R, θ we can write

$$n = \frac{1 - R}{1 + R - 2\sqrt{R}\cos\theta}$$

$$k = \frac{2\sqrt{R}\sin\theta}{1 + R - 2\sqrt{R}\cos\theta}. \qquad (40)$$

Recall that the complex index of refraction $\hat{N}$ and the complex dielectric constant $\hat{\epsilon}$ are related by

$$\begin{aligned} \hat{N} &= n + ik \\ \hat{\epsilon} &= \epsilon_1 + i\epsilon_2 = \hat{N}\hat{N} = (n^2 - k^2) + i2nk. \end{aligned} \tag{41}$$

Thus

$$\begin{aligned} \epsilon_1 &= n^2 - k^2 \\ \epsilon_2 &= 2nk. \end{aligned} \tag{42}$$

Hence, if we measure the reflectance R and determine the phase angle θ through the Kramers-Kronig method to be described we can then obtain all the optical constants of interest.

In order to apply the K-K analysis we consider the logarithm of the reflectivity, a complex function as indicated in the last section which has been shown to satisfy the requirements for dispersion analysis to be valid

$$\ln \hat{r}(\omega) = \ln r(\omega) + i\theta(\omega). \tag{43}$$

Applying the dispersion relation to the real and imaginary parts of this function we have

$$\theta(\omega_o) = \frac{1}{\pi} \int_0^\infty \ln \left| \frac{\omega + \omega_o}{\omega - \omega_o} \right| \frac{d \ln r(\omega)}{d\omega} \, d\omega. \tag{44}$$

The physical measurement gives the reflectance in some interval (a,b) as indicated schematically in Figure 10.

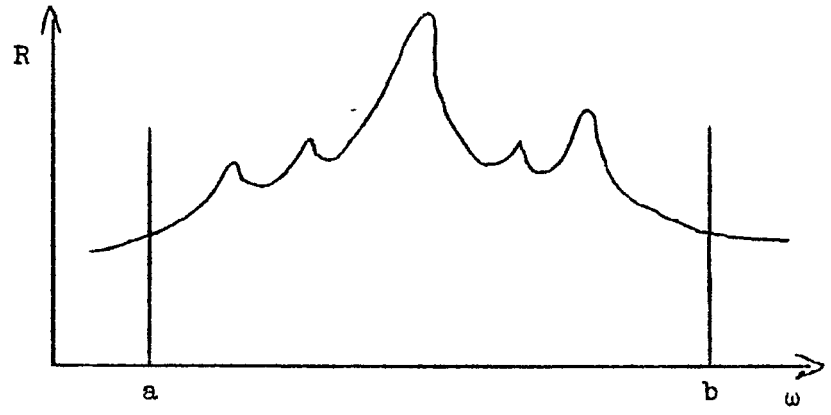

Fig. 10. Typical reflectance spectrum of a solid.

We can write the integral as the sum of three parts

$$\theta(\omega_o) - \int_o^a + \int_a^b + \int_b^\infty = \alpha + \phi + \beta \tag{45}$$

where by using partial integration and the generalized mean value theorem we have

$$\alpha = \frac{1}{\pi} \int_o^a = \frac{1}{\pi} [\ln r(a) - \ln r(\zeta)] \ln \frac{a + \omega_o}{a - \omega_o} = A \ln \left(\frac{\omega_o + a}{\omega_o - a}\right) \tag{46}$$

where $A = \frac{1}{\pi} [\ln r(a) - \ln r(\zeta)]$ $\qquad a \leq \zeta \leq b.$

Similarly

$$\beta = \frac{1}{\pi} \int_b^\infty = B \ln \left(\frac{b + \omega_o}{b - \omega_o}\right) \tag{47}$$

$$B = \frac{1}{\pi} [\ln r(\eta) - \ln r(b)] \qquad a \leq \eta \leq b.$$

As argued in the preceding section A and B are approximately independent of ω_o for diamond although as pointed out strictly speaking $\zeta = \zeta(\omega_o)$, $\eta = \eta(\omega_o)$.

Choosing two frequencies (ω_1 and ω_2) at which we know the crystal is transparent ($k = 0 \rightarrow \theta = 0$) then

$$\begin{aligned} A \ln\left(\frac{\omega_1 + a}{\omega_1 - a}\right) + \phi(\omega_1) + B \ln\left(\frac{b + \omega_1}{b - \omega_1}\right) &= 0 \\ A \ln\left(\frac{\omega_2 + a}{\omega_2 - a}\right) + \phi(\omega_2) + B \ln\left(\frac{b + \omega_2}{b - \omega_2}\right) &= 0 \end{aligned} \tag{48}$$

giving

$$\begin{aligned} A &= \frac{\phi_2 \ln(b, \omega_1) - \phi_1 \ln(b, \omega_2)}{\ln(a, \omega_1) \ln(b, \omega_2) - \ln(a, \omega_2) \ln(b, \omega_1)} \\ B &= \frac{\phi_2 \ln(a, \omega_1) - \phi_1 \ln(a, \omega_2)}{\ln(a, \omega_2) \ln(b, \omega_1) - \ln(a, \omega_1) \ln(b, \omega_2)} \end{aligned} \tag{49}$$

where

$$\ln(x,y) = \ln \frac{x + y}{x - y}$$

Now the values of ω_1, ω_2, ω_o are such that

$$a < \omega_1, \omega_2, \omega_o < b$$

We need now to evaluate the measured contribution ϕ. In order to avoid the singularity at $\omega = \omega_o$ we write

$$\phi(\omega_o) = \frac{1}{\pi}\int_a^b \ln\left|\frac{\omega + \omega_o}{\omega - \omega_o}\right| \frac{d \ln r}{d\omega}\, d\omega$$

$$= \lim_{\varepsilon \to o} \left| \int_a^{\omega_o - \varepsilon} + \int_{\omega_o + \varepsilon}^b \right| \tag{50}$$

Consider the first portion of the integral

$$\int_a^{\omega_o - \varepsilon} \qquad \text{where } \omega < \omega_o$$

and let

$$\omega/\omega_o = x \ (<1)$$

then we can make a series expansion

$$\frac{1}{\pi} \ln \left|\frac{\omega + \omega_o}{\omega - \omega_o}\right| = \frac{1}{\pi} \ln \left(\frac{1 + x}{1 - x}\right) = \frac{1}{\pi} 2\left(x + \frac{1}{3}x^3 + \frac{1}{5}x^5 + \ldots\right) \tag{51}$$

since $|x| \leq 1$.

If we now define $\phi(x) - \frac{2}{\pi}\left(x + \frac{1}{9}x^3 + \frac{1}{25}x^5 + \ldots\right)$

then

$$x \frac{d}{dx}\Phi\,(x) = \frac{2}{\pi}\left(x + \frac{x^3}{3} + \frac{x^5}{5} + \ldots\right)$$

$$= \frac{1}{\pi} \ln \left(\frac{1 + x}{1 - x}\right) = \frac{1}{\pi} \ln \left|\frac{\omega + \omega_o}{\omega - \omega_o}\right| \tag{52}$$

and thus $\frac{1}{\pi}\int_a^{\omega_o - \varepsilon} = \frac{1}{\pi}\int_a^{\omega_o - \varepsilon} x \frac{d\phi}{dx}\, d \ln r$

but $\frac{x}{dx} = \frac{1}{d\,\frac{\omega}{\omega}} = \frac{1}{d \ln \omega}$.

Hence we can write this portion of the integral as

$$\lim_{\varepsilon \to o} \int_a^{\omega_o - \varepsilon} = \int_{\frac{a}{\omega_o}}^{\frac{\omega_o - \varepsilon}{\omega_o}} d\Phi\,(x)\ \frac{d \ln r}{d \ln \omega}. \qquad (53)$$

Similarly consider the portion of the integral where $\omega > \omega_o$, let

$\frac{\omega_o}{\omega} = x'\ (< 1)$.

$$\text{Then } \frac{1}{\pi}\int \ln \left|\frac{\omega + \omega_o}{\omega - \omega_o}\right| \frac{d \ln r}{d\omega}\, d\omega$$

$$= \frac{1}{\pi}\int \ln \left|\frac{1 + x'}{1 - x'}\right| d \ln r = \frac{1}{\pi}\int \ln \frac{1 + x'}{1 - x'}\, d \ln r$$

$$= \frac{1}{\pi}\int x' \frac{d\phi}{dx'}\, d \ln r \qquad (54)$$

$$\frac{x'}{dx'} = \frac{\omega_o}{\omega} \cdot \frac{1}{\omega_o(\frac{d\omega}{\omega^2})}$$

$$= -\frac{\omega}{d\omega} = -\frac{1}{d \ln \omega}.$$

We can thus combine the two portions of the integral

$$\int_{a/\omega_o}^{\omega_o - \varepsilon} d\,\Phi(x)\ \frac{d\ln r}{d\ln\omega} - \int_{\omega_o}^{b/\omega_o + \varepsilon} d\,\Phi(x)\ \frac{d\ln r}{d\ln\omega}. \tag{55}$$

To obtain a single formula for all ω_o we proceed as follows. We note that in the limit as $\omega \to \omega_o$, the function Φ approaches $\frac{\pi}{4}$, i.e.,

$$\lim_{x \to 1} \Phi(x) = \lim_{x \to 1} \frac{2}{\pi}\left(x + \frac{x^3}{9} + \ldots\right) = \frac{\pi}{4}. \tag{56}$$

We can thus ensure continuity of $\Phi(x)$ at $\omega = \omega_o$ by defining a function $\psi(x)$ such that

$$\begin{aligned} \psi(x) &= \Phi(x) && \omega < \omega_o \\ &= \frac{\pi}{4} && \omega = \omega_o \\ &= \frac{\pi}{2} - \Phi(x) && \omega > \omega_o. \end{aligned} \tag{57}$$

We now have our integral in the form

$$\Phi = \int_{f(a)}^{f(b)} \frac{d\ln r}{d\ln\omega}\ d\psi(x). \tag{58}$$

It has been found that for small values of x we can take the first four terms in the series as an accurate representation of our function but for values of x near one a more rapidly converging series must be used.

Bode[30] has given the following functions which we will use with a value of x - .414 taken as the transition between the two series representations.

$\omega < \omega_o$

$$\psi(x) = \frac{2}{\pi}\left(x + \frac{1}{9}x^3 + \frac{1}{25}x^5 + \ldots\right)$$

$$0 < x < 0.414 \qquad (59)$$

$$= \frac{\pi}{4} - \frac{1}{\pi} \ln x \ln y - \frac{2}{\pi}\left(y + \frac{y^3}{9} + \ldots \frac{y^{13}}{169}\right)$$

$$0.414 < x < 1$$

where $y = \frac{1 - x}{1 + x}$

and define

$\omega = \omega_o$

$$\psi(x) = \frac{\pi}{4} \qquad (60)$$

$\omega > \omega_o$

$$\psi(x) = \frac{\pi}{2} - \frac{2}{\pi}\left(x + \frac{x^3}{9} + \ldots \frac{x^{13}}{169}\right)$$

$$0 < x < 0.414$$

$$= \frac{\pi}{4} + \frac{1}{\pi} \ln x \ln y - \frac{2}{\pi}\left(y + \frac{y^3}{9} + \ldots \frac{y^{13}}{169}\right) \qquad (61)$$

$$0.414 < x < 1.$$

For computer calculation we will approximate the integral by summing over a number of finite changes.

$$\Phi = \int_a^b \frac{d \ln r}{d \ln \omega} d\Phi = \sum_i \frac{\Delta \ln r_i}{\Delta \ln \omega_i} \Delta \psi_i(x) \tag{62}$$

$$- \sum_i \frac{\ln r_{i+1} - \ln r_i}{\ln \omega_{i+1} - \ln \omega_i} (\Delta \psi_{i+1} - \Delta \psi_i).$$

The actual computer program is given in Appendix A.

In summary then we proceed as follows. We first measure the reflection at various frequencies

$$\omega_1 \quad \omega_2 \quad \omega_3 \quad \omega_4 \quad \omega_5 \cdots\cdots \omega_N \text{ (eV)}$$

$$R_1 \quad R_2 \quad R_3 \quad R_4 \quad R_5 \cdots\cdots R_N \text{ (\%)}.$$

We calculate the phase angle θ using the method indicated in the preceding discussion

$$\theta_i = \alpha_1 + \phi_i + \beta_i$$

$$\alpha_i = A \ln \left(\frac{\omega_i + a}{\omega_i - a}\right) \quad i = 1, \ldots N \tag{63}$$

$$\beta_i = B \ln \left(\frac{b + \omega_i}{b - \omega_i}\right)$$

where A,B are determined from setting $\theta = 0$ at the non-absorbing frequencies ω_1 and ω_2. From the computed phase angle θ and the measured reflectance R we can determine the optical constants

$$
\begin{aligned}
n_i &= \frac{1 - R_i}{1 - 2\sqrt{R_i}\cos\theta_i + R_i} \\
k_i &= \frac{2\sqrt{R_i}\sin\theta_i}{1 - 2\sqrt{R_i}\cos\theta_i + R_i} \\
\epsilon_{1i} &= n_i^2 - k_i^2 \\
\epsilon_{2i} &= 2 n_i k_i .
\end{aligned}
\tag{64}
$$

We are also interested in the negative imaginary part of the inverse of the complex dielectric function

$$
-\operatorname{Im}\frac{1}{\hat{\epsilon}_i} = \frac{2 n_i k_i}{n_i^2 - k_i^2} \tag{65}
$$

which is related to the electron energy loss which occurs when low energy electrons impinge upon a solid. This will be discussed more fully in the section on results and discussion.

V. RESULTS AND DISCUSSION

Normal incidence reflection measurements on polished Type I and cleaved and polished Type IIa diamonds were made at liquid nitrogen temperature over the range from 5.5 - 11 eV. Additional room temperature measurements were performed on all but the polished Type IIa specimen from 5.5 - 31 eV. From the reflection data the phase angle of the reflectivity, the components of the complex index of refraction and dielectric function, and the energy loss function were calculated using Kramers-Kronig techniques. The resulting structure in ϵ_2 and $-\mathrm{Im}\,\frac{1}{\tilde{\epsilon}}$ was then assigned according to existing energy band calculations.

Measurements on the three diamond samples were taken at near normal incidence (11°) using a glass light pipe coated with sodium salicylate, which could be rotated to monitor the incident and reflected beams. Measurements were made on diamond surfaces both "as received" and after an acetone-methanol rinse. In some cases a mild sample bake (12 hours at 140°C) was carried out. In the low temperature region all preparations gave essentially the same results, although this was not true for the high energy room temperature results. More details concerning this point will be given later. All diamond samples were supplied by Dr. F. A. Raal of the Diamond Research Laboratory, Crown Mines, Johannesburg, South Africa.

Low temperature data averaged from three separate runs from 5.5 to 11.5 eV on a Type IIa cleaved sample are shown in Figure 11. The features of interest for this region of the spectra are the appearance

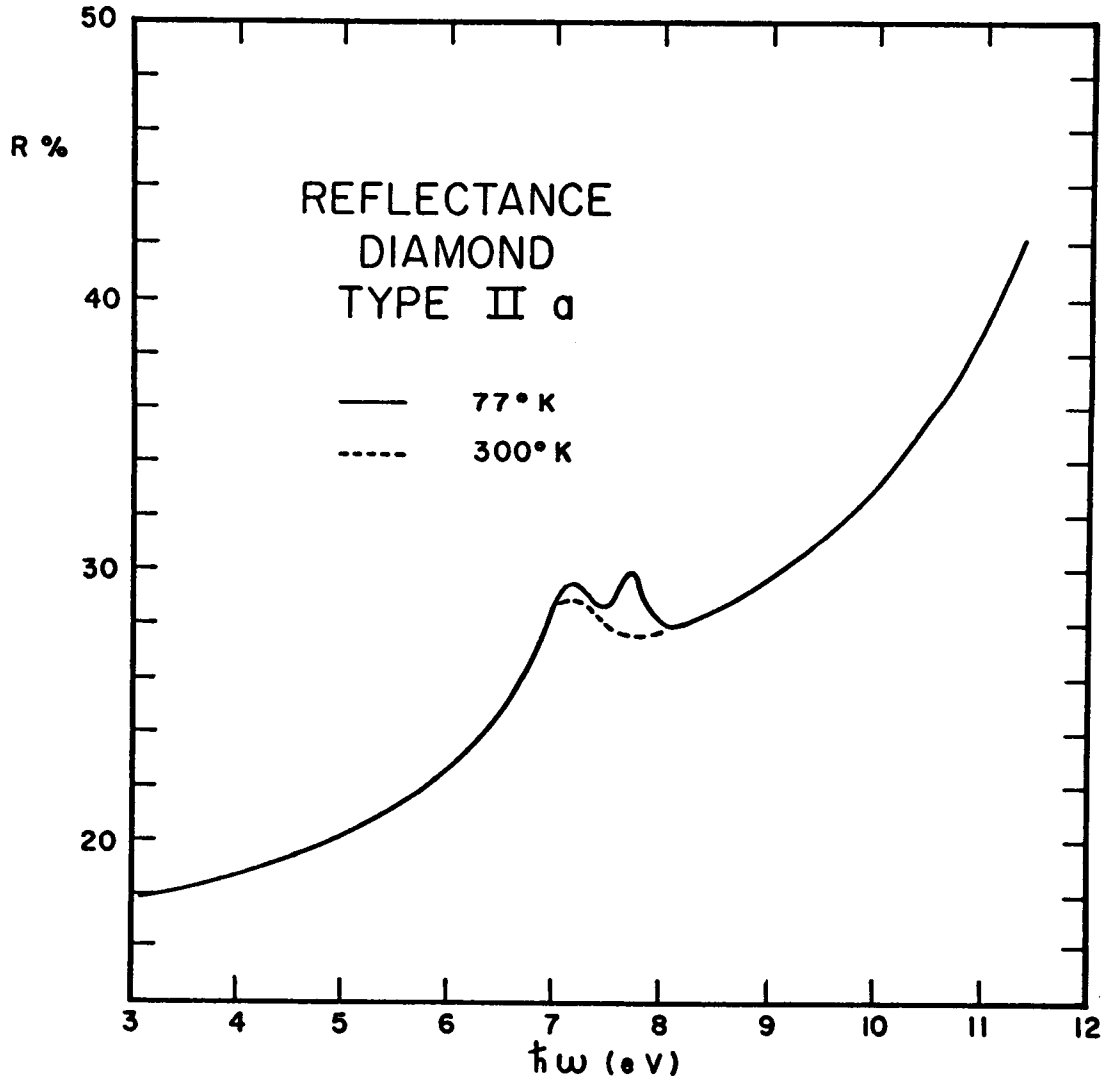

Fig. 11. Reflectance spectra of a cleaved Type IIa diamond at room and liquid nitrogen temperatures.

of a new 7.6 eV peak at low temperature and the lack of structure between 8 - 9 eV. These same features were observed in all samples tested, although the 7 eV peak appears only weakly in a polished Type IIa sample. It is felt that the data obtained from the cleaved Type IIa sample best represent intrinsic diamond properties in this region because of its lower impurity content compared to other diamond types and the general superiority of cleaved over polished surfaces in displaying reflection fine structure. The 7.6 eV peak at low temperature was consistently seen in all specimens studied. The reflectance curve from 5.5 to 11.5 eV was obtained from about 60 data points taken with an average energy separation of 0.05 eV in the critical region of the two peaks. The experimental scatter on any one run was within 1%. The reflectance below 5.5 eV was calculated from existing index of refraction data[1] and matched the present low energy data extremely well. In Figure 12 the low temperature reflectance data is compared in detail with that of Clark, Dean and Harris[16] (CDH).

The significant features of the low temperature data of CDH are the large sharpening of the peak near 7 eV and the drop in reflectance on the high energy side of the peak below that at room temperature. In the present low temperature data only a slight sharpening of the 7 eV peak was seen and in no instance was a drop in reflectance below that at room temperature observed. In the initial stages of this work considerable difficulty was experienced in keeping the surface clean at low temperature. Before replacing a sliding seal between the reflectometer and monochromator by a permanent window, considerable decrease

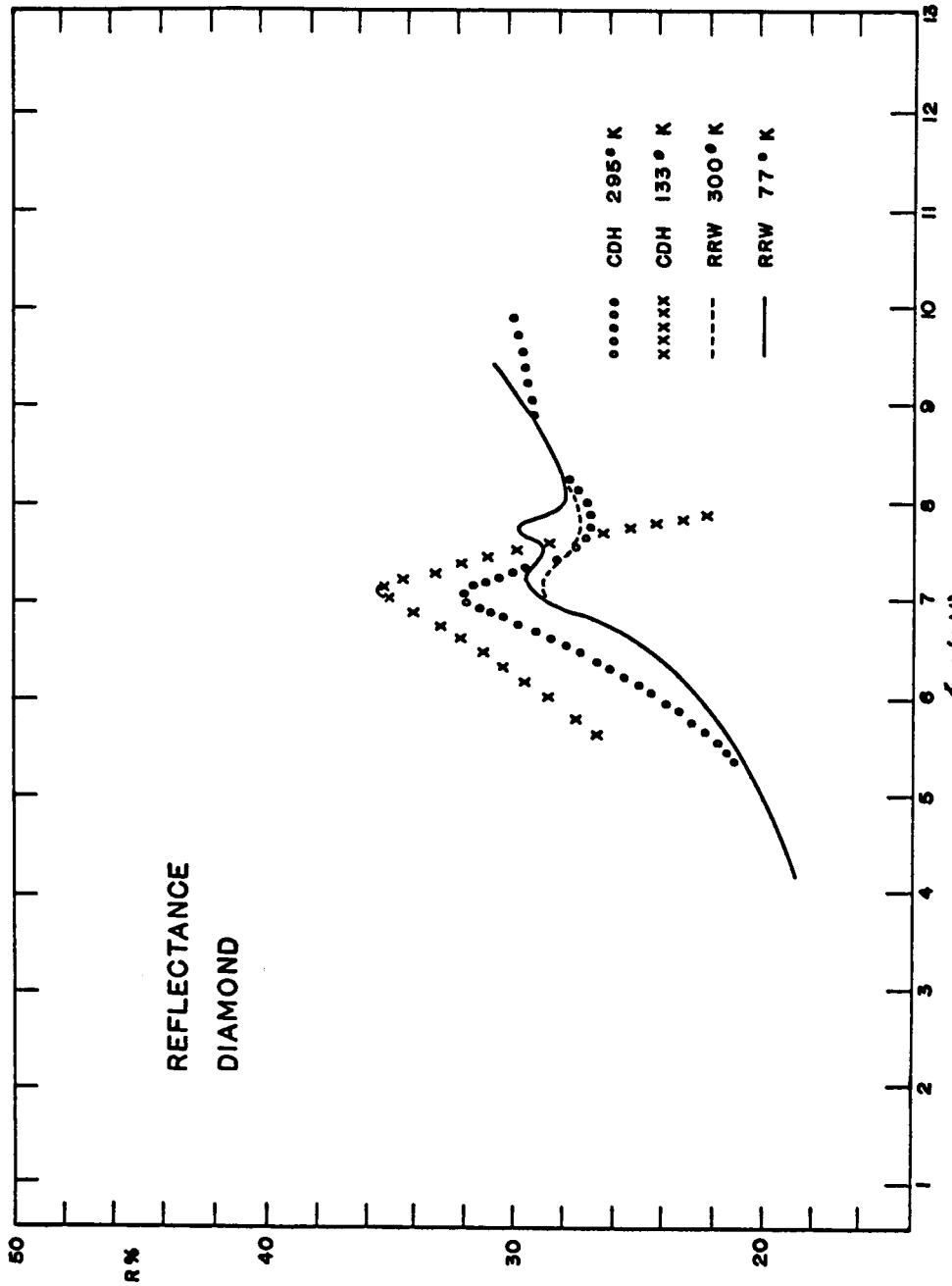

Fig. 12. Detailed comparison of reflectance spectra near 7 eV obtained by Clark, Dean and Harris (CDH) and Roberts, Roessler and Walker (RRW).

in reflectance was observed with time after sample cooling. Similar behavior may explain the decrease of reflectance observed by CDH who used an oil diffusion pumped system. Phillips[18] has interpreted the data of CDH as due to a hybrid exciton at the center of the Brillouin zone. Consistent with this view he considered the drop in low temperature reflectance as the start of an antiresonance and assumed the low temperature curve would display a minimum and rejoin the room temperature value near 8.3 eV. On the basis he placed this direct interband edge $\Gamma_{25'} \rightarrow \Gamma_{15}$ at 8.7 eV. The lack of an antiresonance in the present data casts some doubt on the hybrid exciton interpretation.

Indeed the present data seem more consistent with the earlier interpretation which attributes the 7 eV structure to a near degeneracy of M_0 and M_1 critical points in the vicinity of the Γ point.[1,15] With this interpretation the 77°K data of Figure 12 places the M_0 edge corresponding to the direct $\Gamma_{25'} \rightarrow \Gamma_{15}$ transition at 7.2 eV. The weak temperature dependence of the 7.2 eV peak; i.e., the lack of any appreciable sharpening or energy shift of the peak with temperature, would seem to indicate that an exciton is not responsible for this structure. The fact that a peak rather than a shoulder is observed can be explained if the joint density of states near $\Gamma_{25'} \rightarrow \Gamma_{15}$ falls off fairly rapidly for $\omega > \omega_1$, where ω_1 corresponds to the M_1 edge. The strong temperature dependence of the "new" 7.6 eV peak suggests two possible interpretations. One, that it is due to a near degeneracy of M_1 and M_2 type edges. The recent band calculations of Saslow, Bergstresser and Cohen[11] indicate that such a situation might occur

near the center of the Brillouin zone along the [1,1,1] direction where several critical points exist. Slight temperature shifts in the lattice parameters may cause sufficient changes in the energy bands near this region to introduce one or more strong transitions at 7.6 eV. Note however from Figure 1 that this interpretation does not seem likely if one considers the latest calculation by Herman[12] which does not show complex structure near Γ. Second, that it is an exciton at a point in the Brillouin zone other than the Γ point. There do not, however, appear to be any suitable gaps in the calculations shown in Figure 1 of the necessary energy; i.e., of the order of 8 eV. This point together with the restriction that the direct gap must be less than 7.5 eV[11,27] in order to accommodate both the well established position of the Δ_1 minimum and the identification of the prominent 12.6 eV peak with $X_4' - X_1$, give strong evidence against the second explanation.

The interpretation just given of the reflectance structure in terms of direct transitions should really be given not from the reflectance curve but from the ε_2 spectra. It will be seen, however, that the peaks in ε_2 do indeed occur very close in energy to corresponding peaks in reflectance and the interpretation given is the same.

Additional high energy reflectance data at room temperature were taken for the polished Type I and the cleaved Type IIa diamond specimens. These results combined with those just discussed and previous index of refraction data in the transparent region give a total reflection curve from 1 - 31 eV shown in Figures 13 and 14. Because the room temperature

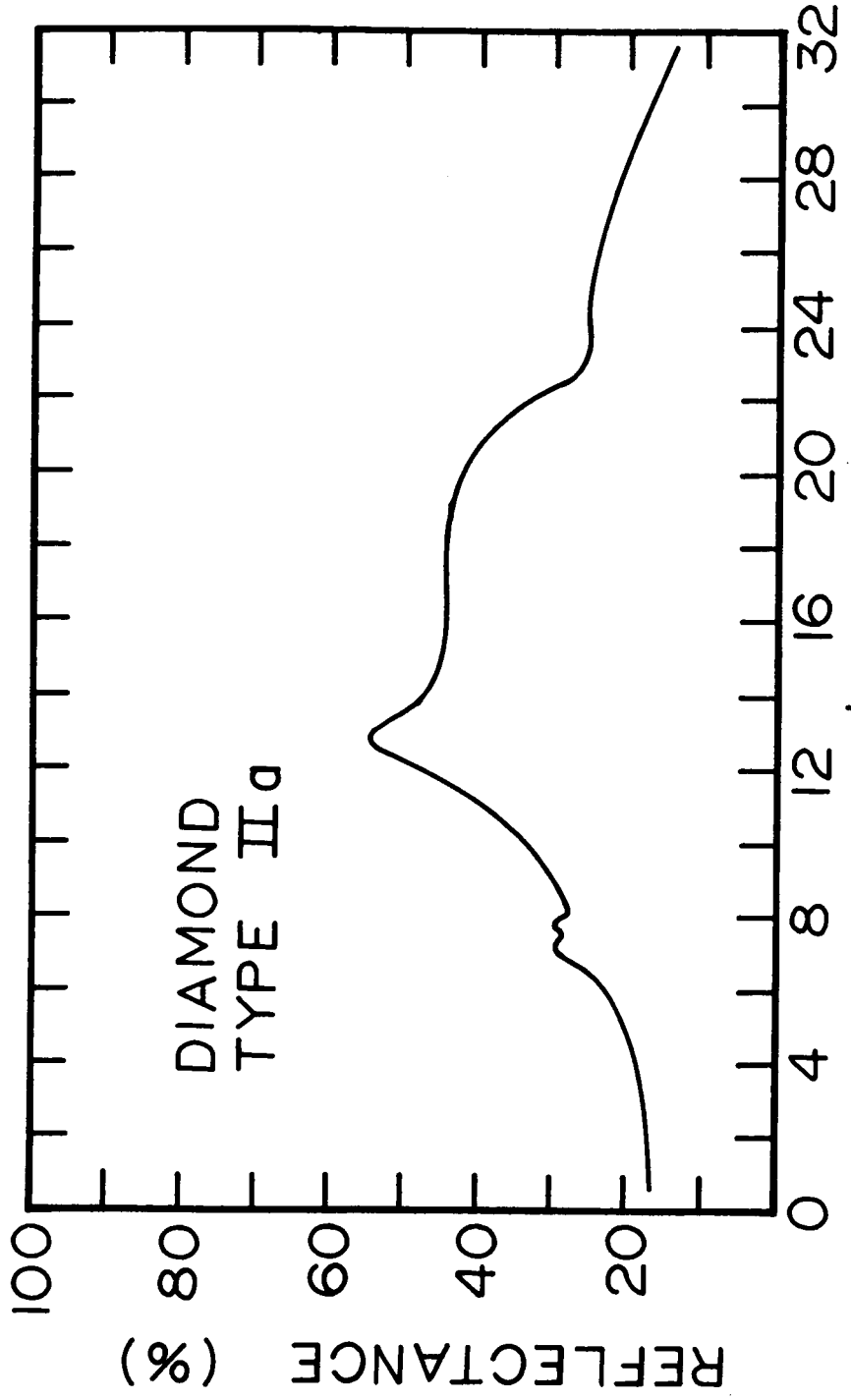

Fig. 13. Reflectance spectrum of a cleaved Type IIa diamond.

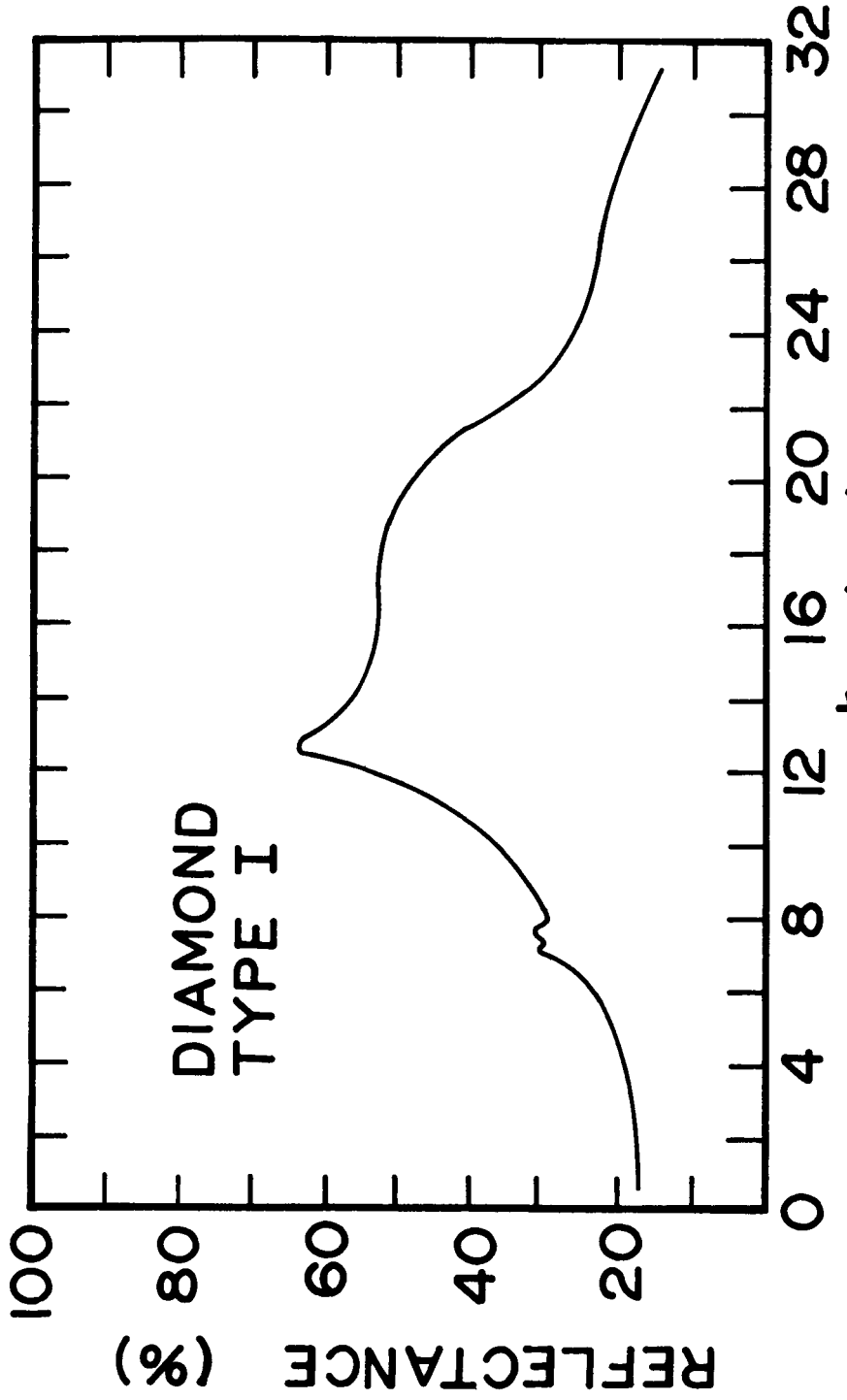

Fig. 14. Reflectance spectrum of a polished Type I diamond.

reflectance matched that at low temperatures for the region from 7.8 eV to the lithium fluoride window cutoff at 11.5 eV it was assumed that the unmeasured low temperature reflectance would also be the same as the measured room temperature results from 11.5 to 31 eV. The large Debye temperature of diamond (~2000°K) supports this observed temperature insensitivity of the high energy structure. With the present apparatus it was not possible to extend the low temperature measurements beyond 11.5 eV since this would require windowless operation and the impurities streaming into the reflectometer from the monochromator would build up on the cold sample surface and give reflectance results not intrinsic to diamond.

From the reflectance curves the phase angle was calculated using the method previously described. A total of 85 reflectance values were used in the computer program to approximate the reflectance curve by a series of short line segments. The density of points chosen was highest in the regions of structure where rapid changes required much shorter line segments in order to better represent the reflectance curves. The actual data points used and the results of the computer calculation for the phase angles of both diamond samples are given in Appendix B.

Once the phase angle was known the other optical constants could be calculated. Figures 15 and 16 show the results for ε_1, ε_2 and $-\mathrm{IM}\,\frac{1}{\tilde{\varepsilon}}$ for the two types of diamond. Calculated results for these quantities as well as n and k are also given in Appendix B.

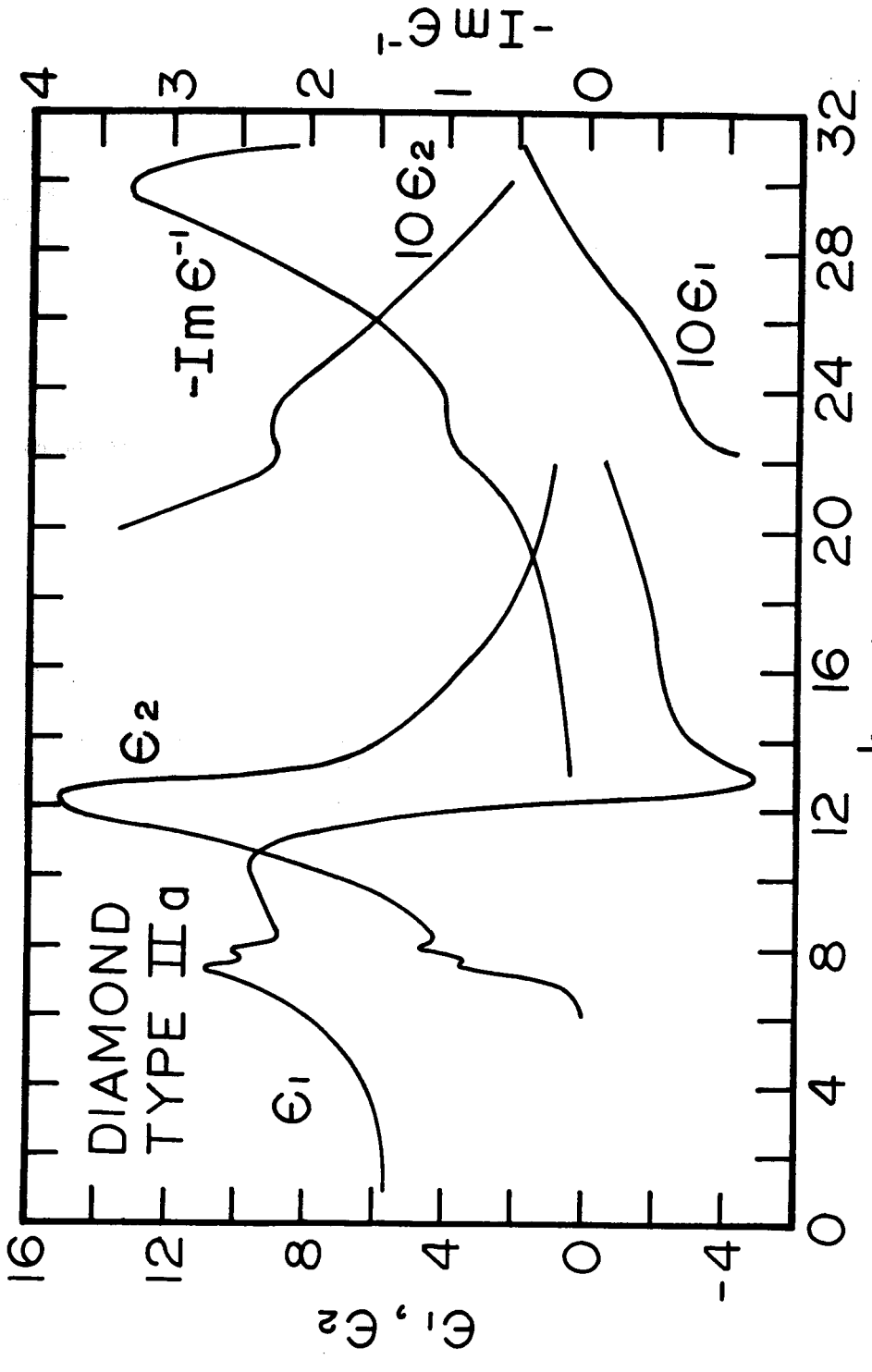

Fig. 15. The real and imaginary parts of the dielectric function and the energy loss function for a cleaved Type IIa diamond.

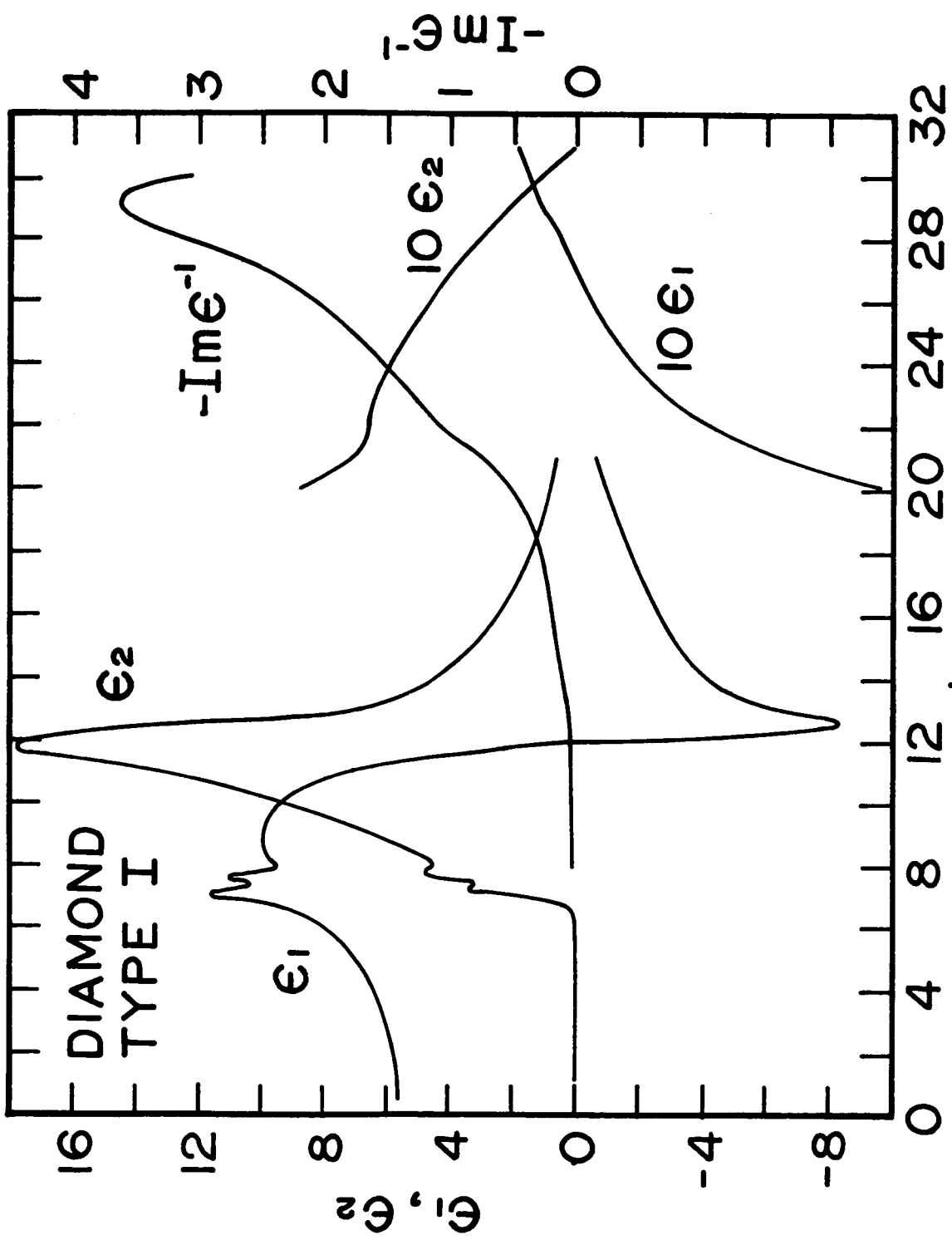

Fig. 16. The real and imaginary parts of the dielectric function and the energy loss function for a polished Type I diamond.

Figure 15 shows the spectrum for ε_2 which is closely related to the joint density of states function. By analogy with silicon the lowest energy direct interband transition is expected to be $\Gamma_{25'} \rightarrow \Gamma_{15}$ and the 7.3 eV peak in ε_2 is assigned to this transition. Note that this peak has been shifted by the integral transform from 7.2 eV in reflectance to 7.3 eV in ε_2 while the peak at 7.6 eV in reflectance has shifted to 7.8 eV. The interpretation of this peak remains the same as given above.

The structure observed by Clark et al.[16] and Roessler[26] near 9 eV did not appear in the present data. This result is in agreement with Philipp and Taft[1,17] and a previous measurement in this laboratory by Walker and Osantowski.[15]

The general shape of ε_2 for diamond, Ge and Si is quite similar in appearance in that the spectrum of each material is dominated by a single large peak. In Ge and Si the energy band gap $X_4 \rightarrow X_1$ was determined by comparing band theory results with reflectivity data. This gap is insensitive to the potential assumed in the band calculation. By an examination of the energy band contour near a critical point the class of edge may be determined. The edge associated with the $(X_4 - X_1)$ critical point is of the M_1 class. Brust[27] has shown for Ge and Si that along the Σ axis there occurs another critical point which belongs to the M_2 class. He thus explains the dominant peak in the ε_2 spectrum of Ge and Si as resulting from two nearly degenerate critical points corresponding to $(X_4 - X_1)$ and $(\Sigma_4 - \Sigma_1)$. We make a similar assignment

for the large peak in diamond at 12.2 eV as arising from nearly degenerate critical points ($X_4 - X_1$) and ($\Sigma_2 - \Sigma_3$) shown in Figure 1.

In the present study no definite sharp structure was observed near 16 eV either in reflectance or in ε_2. However most of the line intensities between 13 and 19 eV were rather unstable and it is possible that such structure does exist within the experimental uncertainty of 5% obtained in this region. It is noted however that the value of ε_2 in the high energy tail of the 12.2 eV peak indicates that a number of transitions are taking place. If one examines the energy band structure calculated by Herman near the X point it is observed that the separation $X_1 \rightarrow X_1$ is near 16 eV and the bands running out from this point along the Σ axis run parallel for a considerable distance which could account for the slow drop off of ε_2 near 16 eV.

There is evidence for structure near 23 eV as a small but definite maximum was observed in reflectance and also in ε_2. This energy corresponds fairly well with the energy difference $L_1 \rightarrow L_1$ or $L_1 \rightarrow L_3$ calculated by Herman which occur near 23 and 24 eV respectively. The symmetry elements at L include inversion which implies that the initial and final states must have opposite parity. This means that these transition are not allowed. However, it may be for $\vec{k}$ values slightly away from L, where the symmetry operations do not include inversion, there are a sufficient number of states available of the correct energy to explain the maximum in ε_2. The only other band energy separation in the neighborhood of 23 eV appearing in Herman's work is $\Sigma_1 \rightarrow \Sigma_1$ which is about halfway along $X \rightarrow \Gamma$.

If one considers the SBC calculation we again find that $L_1 \rightarrow L_1$ is separated by 23 eV but $L_1 \rightarrow L_3$ is more nearly 25 eV. Another possibility however does exist namely $X_1 \rightarrow X_1$ which is near 24 eV.

For an alternative explanation of the 23 eV peak consider the following. Since the 1s core electrons are tightly bound, it is reasonable to assume that all of the optical structure observed in this study is due to valence electrons. For energies of a few tens of electron volts the valence electrons are nearly free and we can thus look for energy losses corresponding to plasma resonance. The plasma frequency ω_p can be estimated using the free electron formula

$$\omega_p = \left(\frac{4\pi ne^2}{m}\right)^{\frac{1}{2}} \tag{66}$$

where n is the appropriate density of electrons. For diamond $\hbar\omega_p = 31$ eV when a density of four free electrons per atom is used. Figure 15 shows a peak in the energy loss function $-\mathrm{Im}\frac{1}{\hat{\epsilon}}$ near 30 eV in good agreement with the free electron formula. Whetten[29] has carried out electron energy loss measurements for diamond and found a dominant peak near 31 eV again in good agreement with the present results. It is important to note that Whetten obtained the peak at different energies depending on various surface treatment. When his system had been baked overnight with no special cleaning of the diamond surface the dominant energy loss is near 23 eV with the 31 eV loss being less prominent. However when hydrogen was admitted to the system and the diamond heated to 700°C for 20 minutes the sample after cooling then gave the dominant loss at 31 eV with the 23 eV peak much reduced. It may well be that the small peak in ϵ_2 at 23 eV is due to a small amount of surface contamination.

It is also important to note that whereas Philipp and Taft[17] chose an extrapolation which would give a prominent peak in $-\mathrm{Im}\frac{1}{\hat{\epsilon}}$ near 31 eV, in the method used in this work the 30 eV peak comes out as a matter of course with no extrapolation of data outside the measured range.

The new results on the Type I sample agree very well with that of Philipp and Taft. This is the first time that good quantitative agreement has been obtained between different observers measuring the same type of diamond. Comparing the plots for ϵ_1 and ϵ_2 of Figure 16 with the results of Philipp and Taft one observes that the only real differences arise near the 7 eV structure in ϵ_2. The doublet structure obtained in the present low temperature measurement at 7.3 and 7.8 eV is seen only as a shoulder in the work of Philipp and Taft. When the Type IIa results are compared with those of Type I one again observes general overall agreement but smaller peak values of ϵ_1 and ϵ_2 occur in the Type IIa specimen. The differences in the two types of diamond could be due to imperfect cleavage of the Type IIa crystal or the higher impurity content in the Type I specimen.

In concluding this section mention should be made of the large quantitative differences between previous reflection measurements on diamond. For example, the maximum of the 12 eV peak was observed to be as high as 65%[17] and as low as 45%.[26] A likely explanation of this difference is indicated by the following observation recorded in the present work. The values of reflectance on the Type I sample shown in Figure 14 were obtained after an overnight bake followed by an immediate reflection measurement. The sample was quickly cooled to room temperature

by pouring small amounts of liquid nitrogen down the sample holder tube and monitoring the sample temperature. Measurements taken shortly after an acetone scrub and methanol rinse of the crystal showed a smaller reflectance than when baked. When the sample was left overnight in the reflectometer after rinsing but without bake, reflection values were even lower. The region of flatness from 15 to 19 eV varied from a value of 55% reflectance for the baked treatment to 48% for the rinsed crystal to 32% for the sample left overnight. It is thus clear that surface preparation is very critical for reflection measurements and can account for much of the previous discrepancy. Diffusion pump oil vapor is the most likely source of this contamination during windowless operation.

VI. SUMMARY AND CONCLUSION

Reflection measurements at both room and liquid nitrogen temperatures have been taken on a polished Type I and both cleaved and polished Type IIa diamond crystals in the range from 5.5 to 11.5 eV. A Vacion pumping system was used in the low temperature work to eliminate oil contamination of the crystal surface. Additional room temperature measurements up to 31 eV were made on the polished Type I and cleaved Type IIa crystals.

Using the reflection results the Kramers-Kronig analysis technique was applied to determine the phase angle of the reflectivity. The other optical constants of interest such as n, k, ϵ_1, ϵ_2, $-\mathrm{Im}\frac{1}{\tilde{\epsilon}}$ were then calculated. Structure in ϵ_1 and ϵ_2 occurring at 7.3, 7.8, 12.2 and 23 eV was observed and assigned to various direct interband transitions according to the available band calculations. The new peak at 7.8 eV was interpreted as due to a possible shifting of the complex energy band structure near the Γ point or as due to an exciton somewhere else in the Brillouin zone.

It is felt that while this work represents a distinct advance over previous studies it does not represent the definitive study of diamond. Because of the problems with unstable light sources there still exists the possibility of fine structure which could yet be resolved. The new 7.8 eV peak presents serious theoretical problems and a careful examination of the 7 eV region using the powerful electroreflectance method could be very rewarding.

From the results for reflectance with various surface conditions alluded to in the text it is believed that knowledge of the crystal surface is the most important aspect of any reflection measurement. These results indicate that very careful studies of the effect of surface preparation on reflectance are necessary and in particular the establishment of valid criteria for determining when the surface is truly characteristic of intrinsic bulk material are needed.

APPENDIX A: COMPUTER PROGRAM

```
// JOB KIM      2401
// OPTION LINK
// EXEC FORTRAN
   10 DIMENSION FREQ(250),REFLEC(250),PSI(250),PHI(250)
   20 READ(1,30) UPPER,XLOWR,PI,N,L,M
   30 FORMAT (F6.3,F8.3,F9.5,I5,2I4)
      DO 40 J=1,N,5
      J1=J+4
   40 READ(1,50) (FREQ(I),REFLEC(I),I=J,J1)
   50 FORMAT (10F8.3)
      DO 106 J=1,N
      REFLEC(J)=REFLEC(J)/100.
  106 CONTINUE
   60 DO 150 I=1,N
   70 DO 105 J=1,N
      IF (FREQ(I)-FREQ(J))80,90,100
   80 XIJ=FREQ(I)/FREQ(J)
      IF (XIJ-0.414) 81,81,82
   81 PSI(J)=0.5*PI-(2./PI)*(XIJ+0.111111111*(XIJ)**3+0.04*(XIJ)**5+0.02
     10408163*(XIJ)**7+0.012345679*(XIJ)**9+0.008264463*(XIJ)**11)
      GO TO 105
   82 YIJ=(1.-XIJ)/(1.+XIJ)
      PSI(J)=0.25*PI+(1./PI)*ALOG(XIJ)*ALOG(YIJ)+(2./PI)*(YIJ+0.11111111
     11*(YIJ)**3+0.04*(YIJ)**5+0.020408163*(YIJ)**7+0.012345679*(YIJ)**9
     2+0.008264463*(YIJ)**11)
      GO TO 105
   90 PSI(J)=0.25*PI
      GO TO 105
  100 XJI=FREQ(J)/FREQ(I)
      IF (XJI-0.414) 101,101,102
  101 PSI(J)=(2./PI)*(XJI+0.111111111*(XJI)**3+0.04*(XJI)**5+0.020408163
```

```
     1*(XJI)**7+0.012345679*(XJI)**9+0.00826446 3*(XJI)**11)
      GO TO 105
102   YJI=(1.-XJI)/(1.+XJI)
      PSI(J)=0.25*PI-(1./PI)*ALOG(XJI)*ALOG(YJI)-(2./PI)*(YJI+0.11111111
     11*(YJI)**3+0.04*(YJI)**5+0.020408163*(YJI)**7+0.012345679*(YJI)**9
     2+0.00826446 3*(YJI)**11)
105   CONTINUE
      PHI(I)=0.0
      N1=N-1
      DO 110 J=1,N1
110   PHI(I)=PHI(I)+(ALOG(SQRT (REFLEC(J+1)))-ALOG(SQRT (REFLEC(J))))*(P
     1SI(J+1)-PSI(J))/(ALOG(FREQ(J+1))-ALOG(FREQ(J)))
150   CONTINUE
      A=(PHI(M)*ALOG((UPPER+FREQ(L))/(UPPER-FREQ(L)))-PHI(L)*ALOG((UPPER
     1+FREQ(M))/(UPPER-FREQ(M))))/(ALOG((XLOWR+FREQ(L))/(FREQ(L)-XLOWR))
     2*ALOG((UPPER+FREQ(M))/(UPPER-FREQ(M)))-ALOG((XLOWR+FREQ(M))/(FREQ(
     3M)-XLOWR))*ALOG((UPPER+FREQ(L))/(UPPER-FREQ(L))))
      B=(PHI(M)*ALOG((XLOWR+FREQ(L))/(FREQ(L)-XLOWR))-PHI(L)*ALOG((XLOWR
     1+FREQ(M))/(FREQ(M)-XLOWR)))/(ALOG((XLOWR+FREQ(M))/(FREQ(M)-XLOWR))
     2*ALOG((UPPER+FREQ(L))/(UPPER-FREQ(L)))-ALOG((XLOWR+FREQ(L))/(FREQ(
     3L)-XLOWR))*ALOG((UPPER+FREQ(M))/(UPPER-FREQ(M))))
160   WRITE (3,170) A,B
170   FORMAT(2F8.3)
      DO 180 I=1,N1
      ALPHA=A*ALOG((FREQ(I)+XLOWR)/(FREQ(I)-XLOWR))
      BETA=B*ALOG((UPPER+FREQ(I))/(UPPER-FREQ(I)))
      ANGLE=-1.*(ALPHA+PHI(I)+BETA)
      XN=(1.-REFLEC(I))/(1.-2.*SQRT (REFLEC(I))*COS (ANGLE)+REFLEC(I))
      XK=(2.*SQRT (REFLEC(I))*SIN (ANGLE))/(1.-2.*SQRT (REFLEC(I))*COS (
     1ANGLE)+REFLEC(I))
      XE1=XN**2-XK**2
```

```
      XE2=2.*XN*XK
      XIME=XE2/(XE1**2+XE2**2)
      ANGLE=ANGLE*180./PI
      REFLEC(I)=REFLEC(I)*100.
  180 WRITE(3,190) FREQ(I),REFLEC(I),ANGLE,XN,XK,XE1,XE2,XIME
  190 FORMAT (1H0,2F9.3,6F10.3)
      CALL EXIT
      END
/*
// EXEC LNKEDT
// EXEC
/*
/+
```

APPENDIX B: COMPUTER RESULTS CLEAVED TYPE IIa DIAMOND

// EXEC

0.005 -0.695

eV	R	θ	n	k	ε_1	ε_2	$-\mathrm{Im}\,\varepsilon^{-1}$
0.620	16.800	-0.038	2.389	-0.002	5.708	-0.008	-0.000
1.240	16.900	0.0	2.396	-0.0	5.741	0.0	0.0
1.860	17.100	-0.017	2.410	-0.001	5.809	-0.003	-0.000
2.480	17.400	-0.090	2.431	-0.004	5.911	-0.019	-0.001
2.730	17.600	-0.146	2.445	-0.006	5.980	-0.031	-0.001
2.980	17.800	-0.160	2.460	-0.007	6.050	-0.035	-0.001
3.220	18.000	-0.207	2.474	-0.009	6.119	-0.046	-0.001
3.470	18.300	-0.230	2.495	-0.011	6.226	-0.052	-0.001
3.720	18.600	-0.184	2.517	-0.009	6.333	-0.043	-0.001
3.970	18.900	-0.126	2.538	-0.006	6.442	-0.030	-0.001
4.220	19.200	-0.117	2.560	-0.006	6.553	-0.029	-0.001
4.460	19.600	-0.090	2.589	-0.004	6.702	-0.023	-0.001
4.710	20.000	0.0	2.618	-0.0	6.854	0.0	0.0
5.000	20.500	0.121	2.655	0.006	7.048	0.034	0.001

5.250	20.900	0.246	2.684	0.013	7.205	0.072	0.001
5.500	21.400	0.262	2.722	0.015	7.407	0.080	0.001
5.750	22.000	0.242	2.767	0.014	7.654	0.078	0.001
6.000	22.800	0.245	2.828	0.015	7.995	0.084	0.001
6.250	23.800	0.392	2.905	0.025	8.438	0.148	0.002
6.500	24.900	0.575	2.991	0.040	8.947	0.239	0.003
6.750	26.700	1.107	3.136	0.085	9.826	0.536	0.006
7.000	28.900	2.807	3.305	0.245	10.864	1.618	0.013
7.050	29.200	3.407	3.321	0.301	10.940	2.001	0.016
7.150	29.500	4.662	3.321	0.416	10.853	2.762	0.022
7.200	29.400	5.238	3.298	0.462	10.660	3.050	0.025
7.250	29.300	5.736	3.276	0.501	10.479	3.284	0.027
7.350	28.800	6.385	3.217	0.539	10.056	3.469	0.031
7.400	28.600	6.472	3.198	0.540	9.938	3.454	0.031
7.500	28.600	6.512	3.197	0.543	9.927	3.473	0.031
7.600	29.200	6.750	3.237	0.581	10.138	3.759	0.032
7.650	29.700	7.218	3.259	0.635	10.221	4.139	0.034

7.700	29.800	7.945	3.240	0.696	10.010	4.512	0.037
7.750	29.600	8.655	3.196	0.743	9.662	4.752	0.041
7.850	28.500	9.212	3.094	0.740	9.028	4.578	0.045
7.950	28.200	9.303	3.070	0.734	8.884	4.507	0.045
8.000	27.800	9.243	3.044	0.714	8.757	4.348	0.045
8.100	27.800	8.959	3.055	0.695	8.849	4.245	0.044
8.500	28.500	9.164	3.096	0.736	9.045	4.560	0.044
9.000	29.500	9.738	3.142	0.819	9.202	5.146	0.046
9.500	31.300	10.452	3.231	0.955	9.527	6.168	0.048
10.000	33.500	11.545	3.311	1.154	9.633	7.639	0.051
10.500	36.200	12.972	3.369	1.426	9.315	9.610	0.054
11.000	39.500	14.862	3.360	1.790	8.083	12.031	0.057
11.500	43.300	17.286	3.214	2.217	5.418	14.253	0.061
12.000	48.000	20.538	2.850	2.665	1.024	15.191	0.066
12.500	53.000	25.079	2.225	2.922	-3.585	13.000	0.071
12.600	54.300	26.374	2.053	2.941	-4.434	12.073	0.073
12.700	54.800	27.869	1.890	2.894	-4.802	10.937	0.077
12.800	55.000	29.369	1.748	2.826	-4.931	9.882	0.081

12.900	54.500	30.762	1.647	2.734	-4.760	9.004	0.087
13.000	54.000	31.985	1.568	2.653	-4.581	8.319	0.092
13.500	50.500	36.666	1.356	2.325	-3.568	6.308	0.120
13.750	48.300	38.252	1.321	2.198	-3.088	5.807	0.134
14.000	47.100	39.398	1.289	2.123	-2.846	5.474	0.144
14.500	45.500	41.648	1.219	2.006	-2.537	4.893	0.161
15.000	44.700	43.758	1.149	1.922	-2.373	4.417	0.176
16.000	44.400	48.469	0.992	1.780	-2.185	3.532	0.205
17.000	44.300	53.709	0.850	1.638	-1.960	2.785	0.240
18.000	44.200	59.475	0.728	1.494	-1.702	2.175	0.285
18.500	44.000	62.614	0.675	1.420	-1.560	1.916	0.314
19.000	43.700	65.960	0.627	1.344	-1.414	1.684	0.348
19.500	43.000	69.489	0.587	1.266	-1.257	1.487	0.392
20.000	42.000	73.110	0.556	1.189	-1.104	1.321	0.446
20.500	40.800	76.918	0.529	1.112	-0.957	1.177	0.512
21.000	39.000	80.872	0.512	1.035	-0.809	1.059	0.596
21.250	38.000	82.965	0.504	0.996	-0.737	1.005	0.647

21.500	36.700	85.158	0.500	0.955	-0.661	0.956	0.708
21.750	35.000	87.372	0.502	0.912	-0.580	0.915	0.779
22.250	30.500	90.543	0.528	0.840	-0.426	0.887	0.916
22.500	28.300	91.244	0.549	0.814	-0.362	0.894	0.961
22.700	27.100	91.290	0.563	0.804	-0.329	0.906	0.975
22.900	26.500	91.367	0.570	0.798	-0.312	0.910	0.983
23.100	26.000	91.597	0.574	0.791	-0.296	0.909	0.995
23.300	25.700	91.872	0.576	0.785	-0.285	0.905	1.005
24.000	25.400	94.128	0.562	0.758	-0.258	0.852	1.075
25.000	25.200	99.468	0.528	0.699	-0.210	0.738	1.254
26.000	24.300	106.447	0.497	0.621	-0.139	0.618	1.541
27.000	22.700	114.302	0.477	0.536	-0.060	0.512	1.926
28.000	21.000	123.113	0.462	0.449	0.012	0.414	2.411
29.000	19.100	133.496	0.451	0.354	0.079	0.319	2.953
30.000	17.100	146.418	0.446	0.246	0.138	0.219	3.265
31.000	15.200	165.104	0.445	0.105	0.187	0.094	2.141
31.500	14.000	179.464	0.455	0.004	0.207	0.003	0.078

APPENDIX B: COMPUTER RESULTS POLISHED TYPE I DIAMOND

// EXEC

-0.000 -0.634

eV	R	θ	n	k	ε_1	ε_2	$-\mathrm{IM}\ \varepsilon^{-1}$
0.620	16.800	0.030	2.389	0.001	5.708	0.006	0.000
1.240	16.900	0.0	2.396	-0.0	5.741	0.0	0.0
1.860	17.100	-0.051	2.410	-0.002	5.809	-0.010	-0.000
2.480	17.400	-0.144	2.431	-0.006	5.911	-0.030	-0.001
2.730	17.600	-0.205	2.445	-0.009	5.980	-0.043	-0.001
2.980	17.800	-0.221	2.460	-0.010	6.049	-0.048	-0.001
3.220	18.000	-0.269	2.474	-0.012	6.119	-0.060	-0.002
3.470	18.300	-0.291	2.495	-0.013	6.225	-0.066	-0.002
3.720	18.600	-0.240	2.517	-0.011	6.333	-0.056	-0.001
3.970	18.900	-0.174	2.538	-0.008	6.442	-0.042	-0.001
4.220	19.200	-0.154	2.560	-0.007	6.553	-0.038	-0.001
4.460	19.600	-0.111	2.589	-0.006	6.702	-0.029	-0.001
4.710	20.000	0.0	2.618	-0.0	6.854	0.0	0.0
5.000	20.500	0.156	2.655	0.008	7.048	0.044	0.001

5.250	20.900	0.156	2.684	0.008	7.206	0.045	0.001
5.750	22.000	0.116	2.767	0.007	7.655	0.037	0.001
6.000	22.800	0.023	2.828	0.001	7.996	0.008	0.000
6.250	23.800	0.062	2.905	0.004	8.440	0.023	0.000
6.500	24.900	0.085	2.992	0.006	8.952	0.035	0.000
6.750	26.700	0.261	3.138	0.020	9.848	0.127	0.001
7.000	29.500	1.708	3.370	0.155	11.332	1.043	0.008
7.100	30.400	3.025	3.432	0.287	11.694	1.969	0.014
7.150	30.500	3.809	3.425	0.362	11.602	2.477	0.018
7.200	30.500	4.529	3.408	0.428	11.434	2.916	0.021
7.250	30.300	5.222	3.373	0.485	11.140	3.271	0.024
7.350	29.300	5.759	3.275	0.503	10.473	3.296	0.027
7.400	29.200	5.645	3.270	0.491	10.453	3.211	0.027
7.500	29.300	5.426	3.284	0.476	10.561	3.124	0.026
7.600	30.500	5.684	3.376	0.531	11.112	3.587	0.026
7.650	31.000	6.303	3.396	0.602	11.171	4.087	0.029
7.700	31.100	7.062	3.376	0.672	10.943	4.536	0.032

7.750	30.900	7.736	3.332	0.722	10.584	4.810	0.036
7.850	30.100	8.466	3.241	0.749	9.942	4.855	0.040
7.950	29.400	8.546	3.186	0.727	9.621	4.633	0.041
8.000	29.300	8.407	3.184	0.713	9.630	4.539	0.040
8.100	29.300	8.222	3.191	0.699	9.696	4.460	0.039
8.500	30.600	8.657	3.270	0.785	10.075	5.130	0.040
9.000	32.000	9.849	3.312	0.943	10.082	6.244	0.044
9.500	33.700	11.045	3.357	1.126	10.004	7.564	0.048
10.000	35.800	12.343	3.397	1.353	9.707	9.195	0.051
10.500	38.300	13.751	3.414	1.628	9.004	11.114	0.054
11.000	41.500	15.293	3.397	1.973	7.645	13.406	0.056
11.500	45.800	17.104	3.298	2.422	5.009	15.976	0.057
12.000	52.200	19.655	2.965	3.015	-0.298	17.881	0.056
12.500	62.300	24.990	1.962	3.470	-8.194	13.615	0.054
12.600	63.300	26.792	1.726	3.374	-8.402	11.648	0.056
12.700	63.600	28.492	1.554	3.249	-8.140	10.100	0.060

12.800	63.500	30.069	1.427	3.122	-7.712	8.913	0.064
12.900	63.000	31.488	1.339	3.001	-7.212	8.037	0.069
13.000	62.500	32.787	1.268	2.895	-6.774	7.342	0.074
13.500	58.700	37.634	1.106	2.505	-5.052	5.540	0.099
13.750	57.400	39.428	1.056	2.385	-4.572	5.034	0.109
14.000	56.300	41.071	1.012	2.284	-4.192	4.625	0.119
14.500	54.700	44.062	0.936	2.125	-3.640	3.977	0.137
15.000	54.000	46.915	0.858	2.002	-3.273	3.436	0.153
16.000	53.100	52.817	0.721	1.786	-2.669	2.576	0.187
17.000	52.800	59.049	0.605	1.597	-2.184	1.931	0.227
18.000	52.100	65.813	0.515	1.417	-1.742	1.460	0.283
18.500	51.500	69.419	0.480	1.330	-1.538	1.277	0.320
19.000	50.700	73.166	0.450	1.245	-1.348	1.122	0.365
19.500	49.600	77.077	0.427	1.162	-1.169	0.992	0.422
20.000	48.100	81.109	0.410	1.082	-1.003	0.887	0.495
20.500	46.400	85.386	0.396	1.003	-0.849	0.794	0.588

21.000	43.700	89.830	0.393	0.923	-0.697	0.725	0.717
21.250	42.000	92.083	0.395	0.883	-0.623	0.698	0.797
21.500	40.000	94.251	0.402	0.844	-0.552	0.678	0.887
21.750	37.500	95.979	0.416	0.811	-0.484	0.674	0.978
22.250	34.000	98.632	0.436	0.761	-0.389	0.663	1.121
22.500	32.500	99.754	0.445	0.740	-0.350	0.658	1.184
22.700	31.600	100.636	0.449	0.725	-0.324	0.651	1.230
22.900	30.700	101.586	0.453	0.710	-0.298	0.643	1.279
23.100	29.800	102.469	0.458	0.695	-0.274	0.636	1.326
23.300	29.100	103.341	0.460	0.682	-0.253	0.628	1.371
24.000	26.800	106.574	0.468	0.635	-0.184	0.594	1.536
25.000	24.500	111.437	0.470	0.573	-0.108	0.539	1.784
26.000	23.100	117.145	0.461	0.512	-0.050	0.472	2.095
27.000	22.200	124.512	0.443	0.442	0.001	0.392	2.552
28.000	20.900	133.788	0.429	0.358	0.056	0.308	3.144

29.000	19.300	145.149	0.422	0.262	0.109	0.221	3.638
30.000	17.300	159.535	0.424	0.149	0.157	0.126	3.105
31.000	15.200	179.961	0.439	0.000	0.193	0.000	0.006
31.250	14.700	187.204	0.447	-0.050	0.197	-0.045	-1.100
31.500	14.000	195.837	0.462	-0.110	0.202	-0.102	-1.991
31.750	13.400	206.627	0.484	-0.183	0.201	-0.178	-2.471

REFERENCES

1. H. R. Philipp and E. A. Taft, Phys. Rev. 113, 1002 (1959).

2. J. C. Phillips, J. Phys. Chem. Solids 12, 208 (1960).

3. R. Robertson, J. J. Fox and A. E. Martin, Phil. Trans. A 232, 463 (1934).

4. R. Robertson, J. J. Fox and A. E. Martin, Proc. Roy. Soc. London A 157, 579 (1936).

5. W. Kaiser and W. L. Bond, Phys. Rev. 115, 857 (1959).

6. F. Herman, Phys. Rev. 93, 1214 (1954).

7. C. Herring, Phys. Rev. 57, 1169 (1940).

8. L. Kleinman and J. C. Phillips, Phys. Rev. 116, 880 (1959).

9. L. B. Redei, Proc. Roy. Soc. A 270, 373 (1962).

10. N. V. Cohan, D. Pugh and R. H. Tredgold, Proc. Phys. Soc. 82, 65 (1963).

11. W. Saslow, T. K. Bergstresser and M. L. Cohen, Phys. Rev. Letters 16, 354 (1966).

12. F. Herman, R. L. Kortum, C. D. Kuglin and R. A. Short, International Conference on the Physics of Semiconductors, Kyoto, Japan, Sept. 1966.

13. F. C. Champion, Electronic Properties of Diamond, (London, Butterworth, 1963).

14. H. R. Philipp and E. A. Taft, Phys. Rev. 127, 159 (1962).

15. W. C. Walker and J. Osantowski, Phys. Rev. 134, A153 (1964).

16. C. D. Clark, P. J. Dean and P. V. Harris, Proc. Roy. Soc. A 277, 312 (1964).

17. H. R. Philipp and E. A. Taft, Phys. Rev. 136, A1445 (1964).

18. J. C. Phillips, Phys. Rev. 139, A1291 (1965).

19. C. B. Duke and B. Segall, Phys. Rev. Letters 17, 19 (1966).

20. J. Hermanson, to be published.

21. J. C. Slater, Electromagnetism, (New York, McGraw-Hill, 1947).

22. J. C. Phillips, Solid State Physics, F. Seitz and D. Turnbull, eds., (New York, Academic Press, 1966), Vol. 18.

23. L. Van Hove, Phys. Rev. 89, 1189 (1953).

24. J. C. Phillips, Phys. Rev. 104, 1263 (1956).

25. P. J. Dean, E. C. Lightowlers and D. R. Wright, Phys. Rev. 140, A352 (1965).

26. D. M. Roessler, Optical Properties of Materials in the Far Ultraviolet, Unpublished Ph.D. Thesis, Kings College, London, 1966.

27. F. Herman, (private communication).

28. D. Brust, Phys. Rev. 134, A1337 (1964).

29. N. R. Whetten, Appl. Phys. Letters 8, 135 (1966).

30. H. W. Bode, Network Analysis and Feed-Back Amplifier Design, (New York, Van Nostrand, 1945).